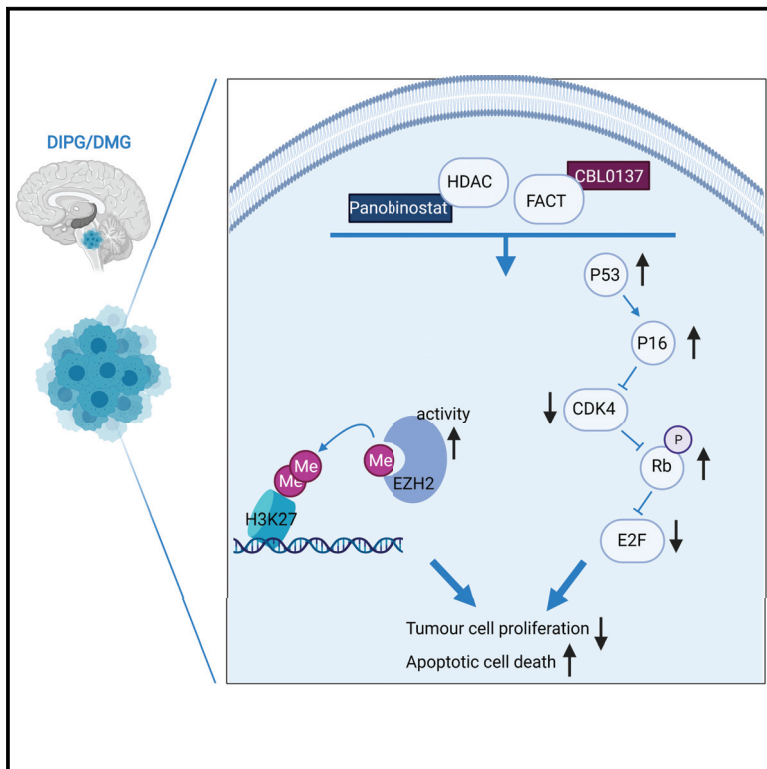Article

Dual targeting of the epigenome via FACT complex and histone deacetylase is a potent treatment strategy for DIPG

Graphical abstract

Authors

Anahid Ehteda, Sandy Simon,
Laura Franshaw, ..., Orazio Vittorio,
Maria Tsoli, David S. Ziegler

Correspondence

mtsoli@ccia.org.au (M.T.),
d.ziegler@unsw.edu.au (D.S.Z.)

In brief

Ehteda et al. find that the histone chaperon FACT is an oncogenic target in diffuse intrinsic pontine glioma. Pharmacological inhibition of FACT with CBL0137 reverses the effect of H3K27M. Co-administration of CBL0137 and panobinostat significantly prolongs survival in two aggressive DIPG *in vivo* models.

Highlights

- CBL0137 inhibits DIPG tumor growth and restores H3K27me3 through FACT inhibition

- Co-administration of CBL0137 and panobinostat enhances survival in DIPG xenografts

- CBL0137 and panobinostat synergistically inhibit the Rb/E2F1 pathway and restore H3K27me3

CellPress

Cell Reports

Article

Dual targeting of the epigenome via FACT complex and histone deacetylase is a potent treatment strategy for DIPG

Anahid Ehteda,[1] Sandy Simon,[1] Laura Franshaw,[1] Federico M. Giorgi,[2] Jie Liu,[1] Swapna Joshi,[1] Jourdin R.C. Rouaen,[1] Chi Nam Ignatius Pang,[3] Ruby Pandher,[1] Chelsea Mayoh,[1,7] Yujie Tang,[4] Aaminah Khan,[1] Caitlin Ung,[1] Ornella Tolhurst,[1] Anne Kankean,[1] Elisha Hayden,[1] Rebecca Lehmann,[1] Sylvie Shen,[1] Anjana Gopalakrishnan,[1] Peter Trebilcock,[1] Katerina Gurova,[5] Andrei V. Gudkov,[5] Murray D. Norris,[1,6] Michelle Haber,[1] Orazio Vittorio,[1,7] Maria Tsoli,[1,7,*] and David S. Ziegler[1,7,8,9,*]

[1]Children's Cancer Institute, Lowy Cancer Research Centre, University of New South Wales, Sydney, NSW, Australia
[2]Department of Pharmacy and Biotechnology, University of Bologna, Bologna, Italy
[3]School of Biotechnology and Biomolecular Sciences, University of New South Wales, Sydney, NSW, Australia
[4]State Key Laboratory of Oncogenes and Related Genes, Key Laboratory of Cell Differentiation and Apoptosis of National Ministry of Education, Department of Pathophysiology, Shanghai Jiao Tong University School of Medicine, Shanghai 200025, China
[5]Department of Cell Stress Biology, Roswell Park Comprehensive Cancer Center, Buffalo, NY, USA
[6]Centre for Childhood Cancer Research, University of New South Wales, Sydney, NSW, Australia
[7]School of Women's and Children's Health, University of New South Wales, Sydney, NSW, Australia
[8]Kid's Cancer Centre, Sydney Children's Hospital, Randwick, NSW, Australia
[9]Lead contact
*Correspondence: mtsoli@ccia.org.au (M.T.), d.ziegler@unsw.edu.au (D.S.Z.)
https://doi.org/10.1016/j.celrep.2021.108994

SUMMARY

Diffuse intrinsic pontine glioma (DIPG) is an aggressive and incurable childhood brain tumor for which new treatments are needed. CBL0137 is an anti-cancer compound developed from quinacrine that targets facilitates chromatin transcription (FACT), a chromatin remodeling complex involved in transcription, replication, and DNA repair. We show that CBL0137 displays profound cytotoxic activity against a panel of patient-derived DIPG cultures by restoring tumor suppressor TP53 and Rb activity. Moreover, in an orthotopic model of DIPG, treatment with CBL0137 significantly extends animal survival. The FACT subunit SPT16 is found to directly interact with H3.3K27M, and treatment with CBL0137 restores both histone H3 acetylation and trimethylation. Combined treatment of CBL0137 with the histone deacetylase inhibitor panobinostat leads to inhibition of the Rb/E2F1 pathway and induction of apoptosis. The combination of CBL0137 and panobinostat significantly prolongs the survival of mice bearing DIPG orthografts, suggesting a potential treatment strategy for DIPG.

INTRODUCTION

Diffuse intrinsic pontine glioma (DIPG) represents the most common form of pediatric high-grade gliomas. DIPG is a highly aggressive childhood malignancy with a median survival of only 9–12 months. Surgical resection is not an option due to its location in the brainstem, and chemotherapy has proven to be ineffective. Currently, radiotherapy is the only standard care that temporarily mitigates the symptoms, delays disease progression, and extends median survival by a few months (Cooney et al., 2017). Therefore, novel and effective therapeutic approaches are urgently needed.

Recent studies have shown that approximately 80% of DIPGs harbor histone H3 mutations at genes encoding histone H3.1 (HIST1H3B) and H3.3 (H3F3A) as a result of the replacement of lysine 27 with methionine (Lewis et al., 2013). This substitution perturbs the methyltransferase activity of the enhancer of zeste

homolog 2 (EZH2) subunit in the polycomb repressive complex 2 (PRC2), leading to disruption of lysine trimethylation at H3 lysine 27 (H3K27me3) and hypomethylation. Subsequent epigenetic dysregulation leading to aberrant transcription is considered to be essential for DIPG oncogenesis (Johung and Monje, 2017; Mohammad et al., 2017). In addition, it was shown that nucleosomes with DIPG-specific histone H3 mutations are less stable with wild-type (Wu et al., 2012). Another genetic aberration frequently observed in DIPG is a loss-of-function mutation in tumor suppressor TP53 in 77% of cases (Schroeder et al., 2014; Schwartzentruber et al., 2012; Sturm et al., 2012). These recent discoveries of genetic alterations in DIPG have revealed important tumorigenic drivers; however, until now there has been no effective strategy to directly target these epigenetic regulators.

Following a high-throughput drug screen, we found that three anti-malarial drugs, i.e., quinacrine, mefloquine, and primaquine,
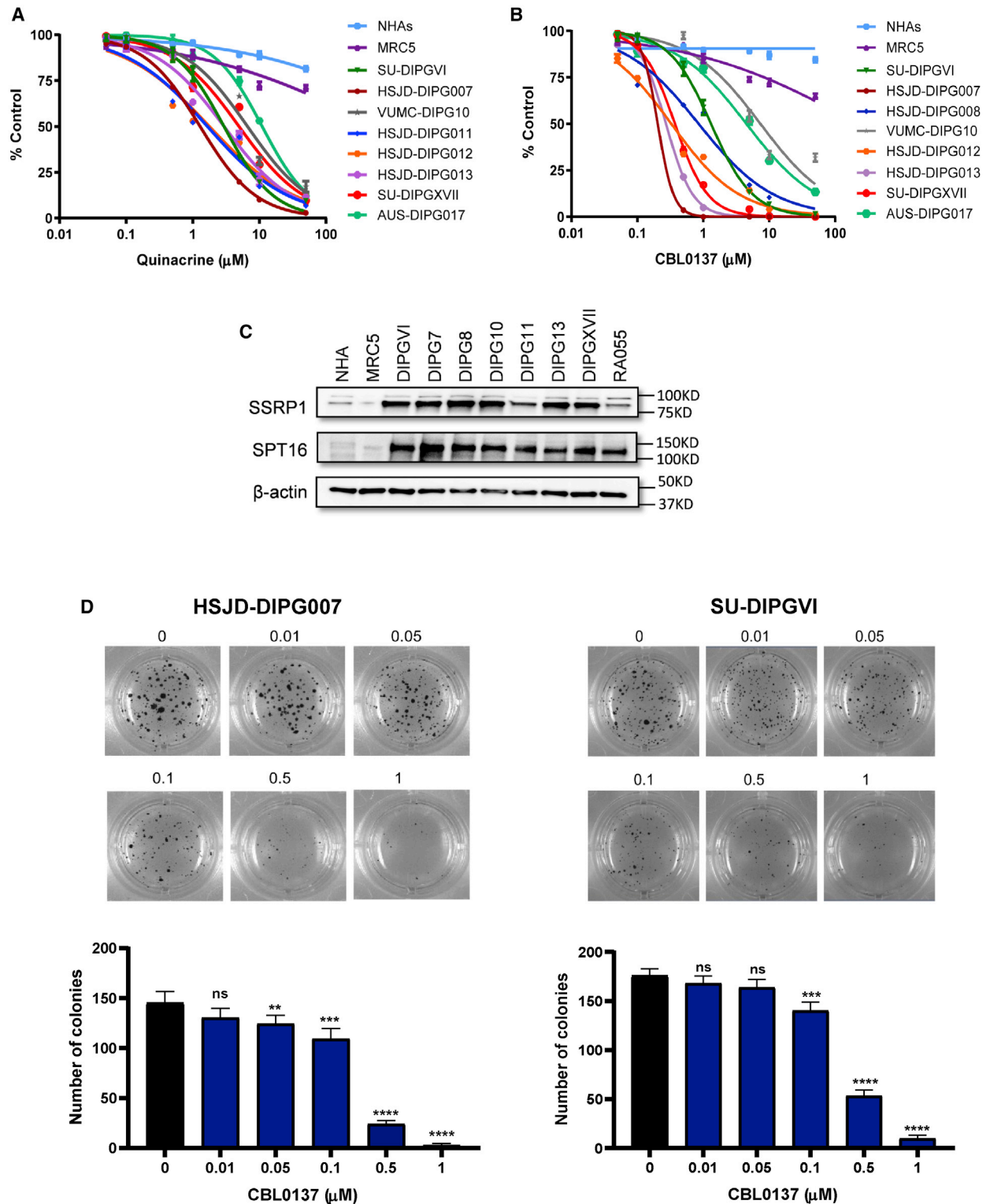
Figure 1. DIPG cells overexpress FACT complex subunits and are sensitive to quinacrine and CBL0317

(A) Patient-derived DIPG cells are sensitive to quinacrine compared to healthy lung fibroblasts (MRC5) and normal human astrocytes (NHAs).

(B) Patient-derived DIPG cells are sensitive to the cytotoxicity effect of CBL0137 compared to MRC5 and NHA cells, with K27M mutant cells showing more sensitivity than the wild-type cells (AUS-DIPG017 and VUMC-DIPG10). Cells were treated for 72 h using various concentrations of CBL0137.

(legend continued on next page)

reduced DIPG cell viability at low micromolar concentrations. CBL0137 is an anti-cancer compound that was modeled on quinacrine and acts by targeting the facilitates chromatin transcription (FACT) complex. FACT is a histone chaperone involved in chromatin remodeling during DNA transcription, replication, and repair. FACT consists of two subunits: structure-specific recognition protein 1 (SSRP1) and suppressor of Ty16 (SPT16) (Gasparian et al., 2011). While FACT is expressed at high levels in the stem or undifferentiated cells, it is not expressed in normal differentiated cells (Garcia et al., 2013). Recent studies have shown that FACT expression is elevated in several cancer types, and its expression is associated with poorly differentiated tumors and low overall survival (Barone et al., 2017; Garcia et al., 2011). It has been demonstrated that CBL0137 activates *TP53* and prevents cellular stress pathways mediated by heat shock factor-1 (HSF-1) and nuclear factor κB (NF-κB) (Gasparian et al., 2011; Neznanov et al., 2009). In pre-clinical models of non-small cell lung carcinoma (NSCLC) (Dermawan et al., 2014), pancreatic cancer (Burkhart et al., 2014), breast cancer (Koman et al., 2012), glioblastoma (GBM) (Barone et al., 2017), and neuroblastoma (Carter et al., 2015), CBL0137 exhibited potent anticancer activity, both as a single agent and when combined with chemotherapeutic agents. CBL0137 has recently completed testing in phase I clinical trials in adults with solid tumors (NCT01905228).

Given that epigenetic dysregulation co-operates with other tumorigenic mutations as the main drivers of DIPG tumor initiation and progression, targeting them simultaneously may be an effective therapeutic strategy. Recently, epigenetic modifying agents have emerged as a promising class of therapeutics for DIPG. Among them, panobinostat, a US Food and Drug Administration (FDA)-approved histone deacetylase inhibitor (HDACi), has been identified as a potent anti-tumor agent against DIPG. Panobinostat induces a dose-dependent increase in both global acetylation and H3K27 trimethylation and is currently in a phase I clinical trial for children with DIPG (NCT02717455) (Grasso et al., 2015; Nagaraja et al., 2017).

In this study, we show that the FACT subunits SSRP1 and SPT16 are overexpressed in DIPG tumors and DIPG cells compared with normal brain tissue and normal human astrocytes. Importantly, we demonstrated that the FACT subunit SSRP1 interacts directly with H3K27M. We have found that CBL0137 upregulates TP53, induces apoptosis, and has profound cytotoxic activity against our panel of DIPG neurosphere cultures. CBL0137 efficiently crosses the blood-brain barrier (BBB) and significantly extends the survival of orthotopic mouse models of DIPG compared with vehicle-treated controls. Combination treatment of CBL0137 and panobinostat synergistically impaired the clonogenic activity of DIPG cells and is proven to be more effective than single-agent treatment in inducing apoptosis and extending the survival in two patient-derived xenograft models of DIPG.

RESULTS

FACT is a therapeutic target in DIPG

We performed a high-throughput drug screening of more than 3,500 compounds at 10 μM concentration from the Library of Pharmacologically Active Compounds (LOPAC), Prestwick, and Tocris libraries to assess their impact on DIPG cell viability. The anti-malarial drugs quinacrine, mefloquine, and primaquine were among the few agents that reduced cell viability below 10% at the concentration of 10 μM (Figure S1A). Further experiments performed with quinacrine showed striking activity with a half-maximal inhibitory concentration (IC$_{50}$) of 2.95 μM. Quinacrine has previously been identified as a potential anti-cancer agent, due to its effects on upregulation of TP53 and inhibition of the NF-κB pathway (Preet et al., 2012). We therefore assessed the activity of quinacrine across a panel of DIPG neurosphere cultures and found consistent sensitivity with an IC$_{50}$ ranging from 1.3 to 2.9 μM (Figure 1A).

Curaxins are a newly identified class of anticancer agents with broad anticancer activity modeled on quinacrine, of which the lead compound in clinical development is CBL0137 (Gasparian et al., 2011). Similar to quinacrine, CBL0137 has been shown to upregulate TP53 activity and inhibit NF-κB-mediated transcription (Gasparian et al., 2011). Therefore, we next evaluated the effect of CBL0137 on the viability of DIPG cultures. CBL0137 exhibited potent cytotoxic activity against a panel of K27M mutant DIPG cells with IC$_{50}$s ranging from 0.2 to 1.3 μM, with minimal effect on human fibroblast cells (MRC5) and normal healthy astrocytes (NHAs). We also found that CBL0137 had a higher IC$_{50}$ in H3K27 wild-type (H3K27WT), suggesting that the H3K27M mutation renders DIPG cells more sensitive to FACT inhibition by CBL0137 (Figure 1B; Tables S1 and S2).

CBL0137 has been shown to target the FACT complex, a histone chaperone involved in chromatin remodeling during DNA transcription, replication, and repair (Gasparian et al., 2011). Histone chaperones are key proteins that regulate multiple steps of nucleosome formation, and their alterations or mutations have been implicated in cancer and other human diseases, but they have not been previously studied in DIPG (Burgess and Zhang, 2013). We therefore evaluated the expression of SSRP1 and SPT16 in a panel of DIPG cells and showed that both SSRP1 and SPT16 proteins were higher in DIPG cultures in comparison with NHAs (Figure 1C). To assess the effect of CBL0137 on DIPG clonogenicity, we performed a soft agar colony formation assay in a range of primary DIPG cultures and showed that the clonogenic activity of DIPG neurospheres was significantly impaired by CBL0137 (Figure 1D). As described earlier, we also found colony formation in the H3K27WT cultures to be less affected by CBL0137 (Figure S1C). Taken together, these results suggest that FACT may be a viable target in DIPG.

To confirm the therapeutic potential of FACT inhibition, we next examined the effect of SSRP1 and SPT16 loss on the

(C) FACT subunits SSRP1 and SPT16 are overexpressed in DIPG cells compared with that in NHAs.
(D) CBL0137 impairs the clonogenic activity of DIPG cells (see also Figure S2C). Data are presented as means ± SD of at least three independent experiments. A one-way ANOVA with Tukey's test was used for comparison between control and CBL0137 groups. **p < 0.01, ***p < 0.001, ****p < 0.0001.
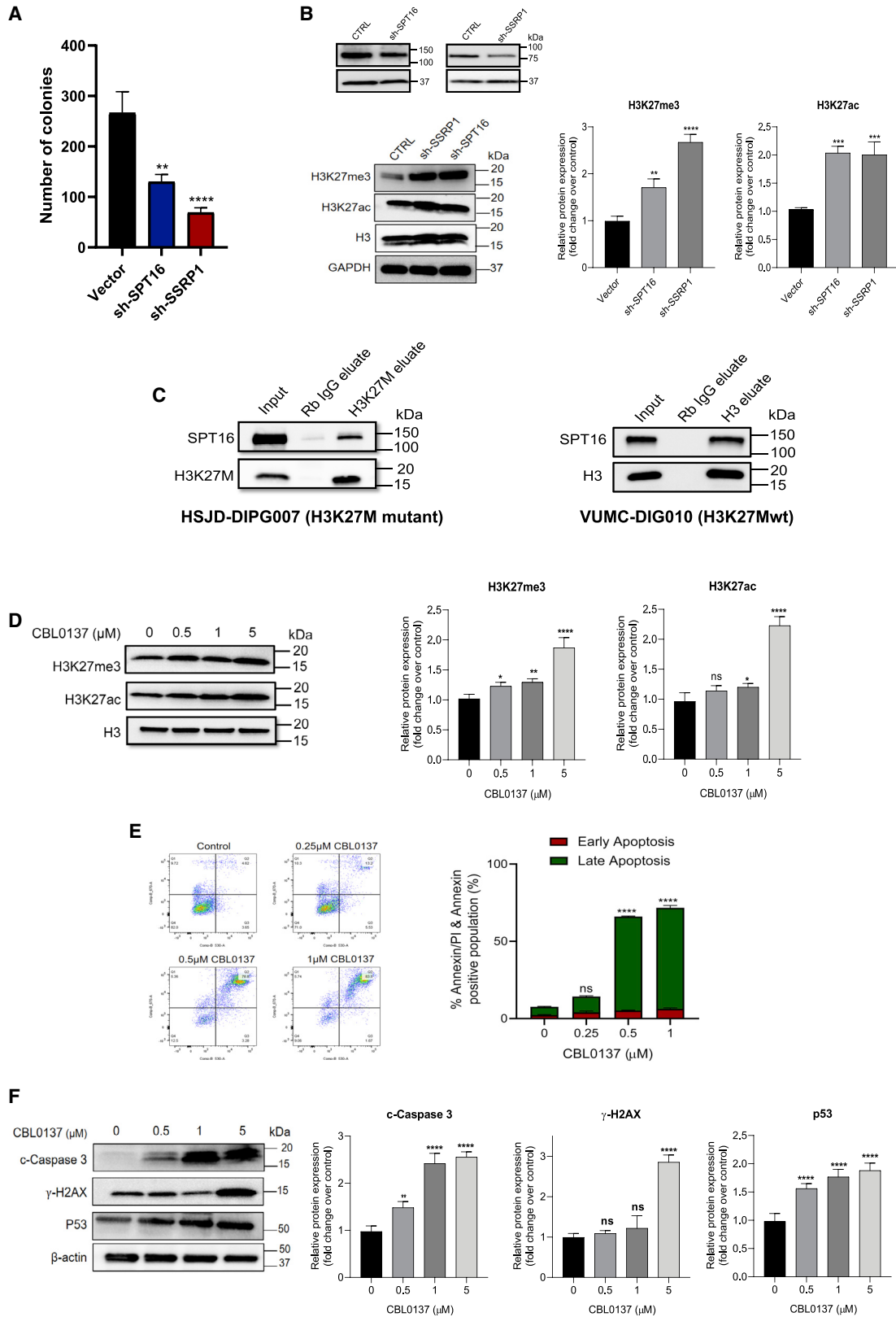
(legend on next page)

clonogenic activity of HSJD-DIPG007 cells through the production of two short hairpin RNA (shRNA) knockdown systems. Independent knockdown of either SSRP1 or SPT16 led to a significant reduction in the number of colonies compared to control (Figure 2A). DIPG tumors that harbor H3K27M mutations are known to exhibit a global reduction in H3K27me3 and a modest increase in acetylated H3K27 (H3K27ac) (Piunti et al., 2017), and H3K27me3 is considered to be a critical target in DIPG. Depletion of SPT16 has been shown to increase H3K27ac levels in embryonic stem cells (Mylonas and Tessarz, 2018). It has also been suggested that polyacetylation of the H3 N-terminal tail results in the rescue of K27M-induced inhibition of PRC2 and reverses the H3K27 hypomethylation phenotype (Brown et al., 2014). We therefore sought to determine whether FACT expression has a direct effect on H3K27 trimethylation and acetylation in DIPG. SSRP1 and SPT16 knockdown each resulted in an increase in H3K27 trimethylation (Figure 2B), suggesting that FACT subunits may regulate post-translational modification of histone H3. Co-immunoprecipitation of SPT16 with H3K27M and H3 also confirmed the direct interaction of SPT16 and the two proteins (Figure 2C). Given the effect of FACT knockdown on epigenetic drivers in DIPG, we next sought to determine whether pharmacological targeting of FACT with CBL0137 leads to a similar effect. We first performed a cytotoxicity assay at various time points to determine the effect of CBL0137 on the viability of DIPG007 cells following 24-h treatment (Figure S1B). We then tested the effect of low concentrations of CBL0137 on H3K27me3 and H3K27ac proteins and showed that CBL0137 increased the level of both the acetylated and methylated forms of the protein in H3K27M mutated cells (Figure 2D; Figure S1D). Taken together, these results suggest that FACT is a promising target in DIPG that directly modulates H3K27M, and that treatment with CBL0137 represents a rational DIPG therapy.

CBL0137 induces apoptosis and DNA damage and modulates p53 level
To determine whether the cytotoxic effect of CBL0137 is due to induction of apoptotic mechanisms in DIPG, we examined key regulators of apoptosis through both flow cytometry analysis and western blotting. To test the effect of CBL0137 on apoptosis, we assessed the levels of annexin V-fluorescein isothiocyanate (FITC) and propidium iodide staining using flow cytometry. HSJD-DIPG007 cell culture was treated with various concentrations of CBL0137 for 48 h. As shown in Figure 2E, the treatment led to a significant induction of apoptosis in HSJD-DIPG007 cells. This result was confirmed by western blot

analysis where CBL0137 treatment resulted in a concentration-dependent increase in cleaved caspase-3. CBL0137 also induced DNA damage in DIPG cells, as shown by increased levels of γ-H2AX (Figure 2F; Figure S1E).

It has been previously shown that FACT inhibition resulted in the modulation of p53 in glioblastoma cells (Gasparian et al., 2011). Somatic loss-of-function mutations in p53 have been identified in 40%–77% of DIPG patients (Grill et al., 2012). Using western blot analysis, we confirmed that CBL0137 treatment led to a concentration-dependent increase in p53 protein level (Figure 2F; Figure S1E). However, the activity of CBL0137 was consistent across a panel of DIPG cultures and independent of TP53 status (Figure 1B; Table S1). We also performed Affymetrix gene expression analysis on HSJD-DIPG007 treated with 0.5 μM CBL0137 for 24 h. Data confirmed that cell cycle and the p53 signaling pathway are the most enriched pathways in Kyoto Encyclopedia of Genes and Genomes (KEGG) pathway enrichment analysis (Table S3).

CBL0137 penetrates the BBB and increases survival in an orthotopic mouse model of DIPG
While we have shown that CBL0137 restores H3K27 trimethylation, induces apoptosis, and inhibits cell proliferation and clonogenicity in DIPG neurosphere cultures, an intact BBB has been identified as a critical reason for the failure of many pharmacological therapies in DIPG. We therefore investigated the brain penetration of CBL0137 using liquid chromatography-tandem mass spectrometry (LC-MS/MS). Following intravenous administration of a single dose of 20 or 50 mg/kg CBL0137, the maximum brain concentrations of the drug (C_{max}) were 5.9 and 45.3 μg/mL, respectively, which were well above the IC$_{50}$ of CBL0137 in DIPG (IC$_{50}$s, 1.125–4.875 μg/mL). The concentration of both 50 and 20 mg/kg CBL0137 in brain tissue and plasma persisted for 24 h after administration, with brain concentrations of CBL0137 more than 50- and 12-fold higher than that in plasma, respectively (Figures 3A and 3B), suggesting the potential for *in vivo* activity and clinical translation. To examine the *in vivo* efficacy of CBL0137, an orthotopic patient-derived xenograft model of HSJD-DIPG007 was used for testing two different dosing schedules. Mice were treated at 4 weeks post-implantation with 50 mg/kg CBL0137 intravenously once a week for 4 weeks (Figure 3C) or 20 mg/kg CBL0137, 5 days on/2 days off for 3 weeks (Figure 3D). With both dose and schedules, we observed a significant prolongation in the survival of the animals (for 50 mg/kg CBL0137, 81 days versus 69.5 days control, p = 0.0120, and for 20 mg/kg CBL0137, 87 days versus 61 days control; p = 0.0013) (Figures 3C and 3D).

Figure 2. FACT inhibition enhances apoptosis and restores p53 and H3K27 trimethylation and acetylation
(A) Knockdown of both FACT subunits impairs the clonogenic activity of HSJD-DIPG007 cells.
(B) Knockdown of the SSRP1 subunit of FACT in HSJD-DIPG007 cells results in an increase in protein expression of H3K27me3 and H3K27ac.
(C) Co-immunoprecipitation of SPT16 with H3K27M in HSJD-DIPG007 cells and H3K27wt in VUMC-DIPG10 cells indicates a direct interaction of SPT16 with mutant and wild-type H3.
(D) CBL0137 restores H3K27 trimethylation and increases H3K27 acetylation in HSJD-DIPG007 cells (24-h treatment) (see also Figure S1D).
(E) CBL0137 induces apoptosis in HSJD-DIPG007 cells in a concentration-dependent manner (see also Figure S1E).
(F) CBL0137 induces caspase-3 cleavage, DNA damage, and p53 protein expression in HSJD-DIPG007 cells (48-h treatment).
Data are presented as means ± SD of at least three independent experiments. Densitometric analysis was performed using ImageJ software. A one-way ANOVA with Tukey's test was used to compare control with CBL0137 groups. **p < 0.01, ***p < 0.001, ****p < 0.0001.
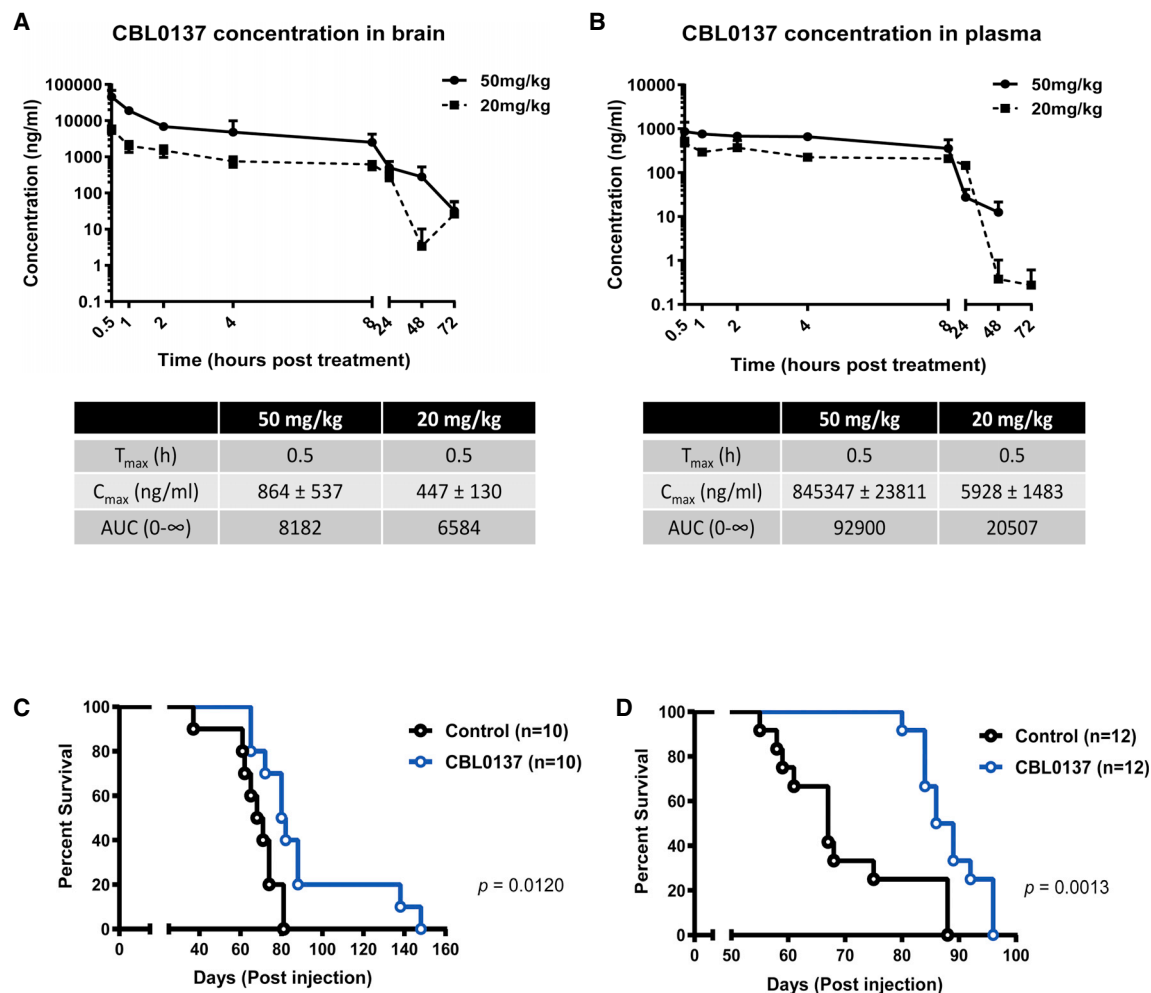
Figure 3. CBL0137 crosses the blood-brain barrier and enhances the survival of an orthotopic model of DIPG
(A and B) Pharmacokinetic analysis of CBL0137 in non-obese diabetic (NOD)/severe combined immunodeficiency (SCID) mice. Mice bearing orthotopic HSJD-DIPG007 xenografts (n = 5/group) were administered with a single dose of (A) 20 or (B) 50 mg/kg CBL0137 intravenously (i.v.). Blood and brain tissues were collected at various time points, and the concentration of CBL0137 was measured by LC-MS/MS. CBL0137 significantly extends survival in the orthotopic mouse model of DIPG. Treatment was commenced 4 weeks after intracranial injection of HSJD-DIPG007 cells.
(C and D) Mice received (C) 50 mg/kg CBL0137 once a week for 4 weeks or (D) 20 mg/kg/day, 5 days on/2 days off for 3 weeks. Median survival for the 50 mg/kg CBL0137-treated group was 81 days versus 69.5 days in the untreated group. For the 20 mg/kg schedule, the median survival of the treated group was 87 days versus and 61 days in the control group. A log-rank (Mantel-Cox) test was used to determine statistical significance between both CBL0137-treated groups compared to vehicle.

FACT inhibition synergizes with HDAC inhibition to suppress DIPG cell growth

Recent therapeutic strategies targeting epigenetic alterations have demonstrated promise in preclinical models of pediatric brain cancer (Hashizume, 2017). These treatment strategies often aim to revert the repressed trimethylation or acetylation phenotype back to an active state to restore normal histone functioning. As epigenetic modifiers, HDACis have shown clinical efficacy in various types of cancers. They inhibit histone deacetylation, thereby facilitating an open chromatin structure and gene activation. Panobinostat is a potent non-selective HDACi that was identified in a chemical screen of patient-derived DIPG cells as having potent anti-tumor activity. (Grasso et al.,

2015). Given the effect of CBL0137 on H3K27 methylation and acetylation, we hypothesized that HDACis such as panobinostat may further potentiate the effect of FACT inhibition. Consistent with our hypothesis, we found that the combination of CBL0137 and panobinostat significantly impaired the clonogenic activity of DIPG cells with combination indices (CIs) indicating a potent synergy at all tested concentrations (Figure 4A; Figure S2A). In order to elucidate whether the FACT complex is a critical factor in the synergistic interaction between CBL0137 and panobinostat, we next examined the effect of SSRP1 and SPT16 loss in combination with panobinostat on the clonogenic activity of HSJD-DIPG007 cells. Independent knockdown of either SSRP1 or SPT16 combined with panobinostat led to a

A

B
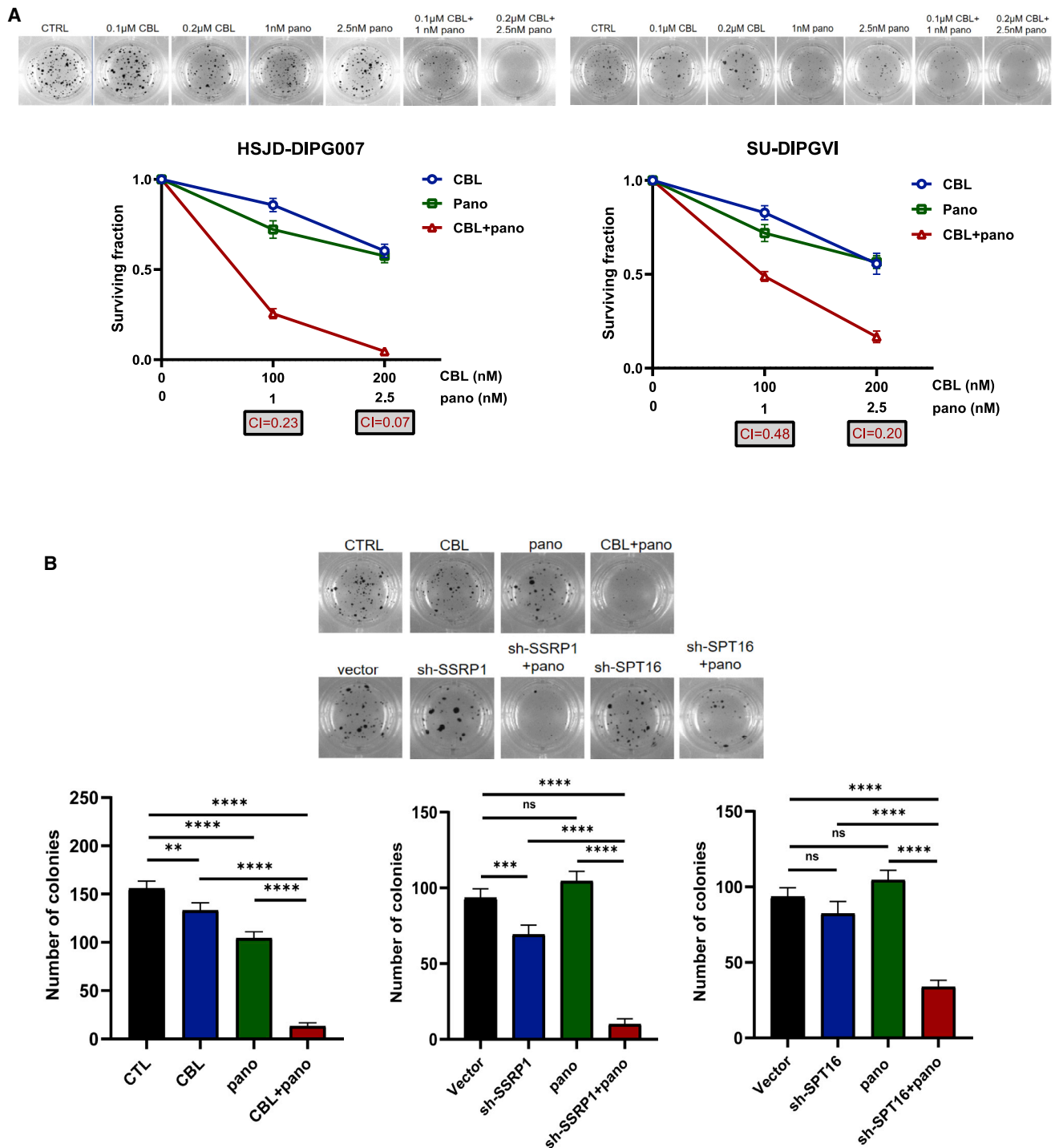
Figure 4. FACT inhibition acts synergistically with panobinostat and reduces clonogenic potential of DIPG cells

(A) CBL0137 and panobinostat synergistically inhibit the clonogenic activity of HSJD-DIPG007 and SU-DIPGVI cells (see also Figure S2A).

(B) Combination of shRNA (sh-)SSRP1 and sh-SPT16 with panobinostat (2.5 nM) results in a significant reduction in the clonogenic activity of HSJD-DIPG007 cells. Combination index (CI) values were calculated using CalcuSyn (Biosoft). Colonies were counted using ImageJ software. Data are presented as means ± SD of at least three independent experiments. A one-way ANOVA with Dunnett's multiple comparison test was used to compare the mean of colony numbers in the combination therapy group with that in single-agent treatments. $**p < 0.01$, $***p < 0.001$, $****p < 0.0001$.

significant reduction in the number of colonies, similar to the effect of the combination of CBL0137 and panobinostat (Figure 4B).

Dual inhibition of FACT and HDAC enhances the expression of apoptotic markers and restores H3K27 trimethylation and acetylation

We next evaluated the effect of combined treatment of the two agents on apoptosis and epigenetic markers. Combination therapy significantly increased the cleavage of both caspase-3 and PARP in HSJD-DIPG007 and SU-DIPGVI cells, indicating that combination therapy induced apoptotic cell death. We also showed that combination therapy increased H3K27 acetylation and H3K27 trimethylation compared with single agent treatment (Figure 5A; Figure S2B). These results were further confirmed by an ELISA assay where significant increases in both H3K27me3 and H3K27ac were observed, with no significant change in global histone methylation and acetylation (Figure 5B).

Combination treatment of CBL0137 with panobinostat affects the Rb/E2F pathway and restores the activity of EZH2

To further elucidate the mechanism of interaction between CBL0137 and panobinostat, we performed an Affymetrix gene expression analysis on HSJD-DIPG007 cells following 24 h of treatment with CBL0137 with and without panobinostat. Results from gene set enrichment analysis (GSEA) identified "Whiteford pediatric cancer markers" and "Hallmark E2F targets" as the two main pathways affected by the combination of CBL0137 and panobinostat (Figure 6A). Whiteford pediatric cancer markers represent the differentially expressed genes in subsets of patient-derived pediatric xenograft tumors compared to the normal tissues. E2F1 is a transcriptional factor that plays a crucial role in controlling the cell cycle, DNA damage checkpoints, and metabolism. E2F is a key target for the growth-suppressing action of retinoblastoma tumor-suppressing protein (Rb), which controls the transition of the G_1 to S phase of the cell cycle (Nevins, 2001). During the cell cycle, Rb is either hyperphosphorylated (inactive) or hypophosphorylated (active). While the phosphorylated form of Rb predominates in proliferating cells, the dephosphorylated form is abundant in differentiating or quiescent cells (Harbour and Dean, 2000). Activated Rb relieves positive regulation of E2F1, which inhibits progression through the G_1 to S phase transition in the cell cycle and represses DNA synthesis and proliferation (Burkhart et al., 2014). To confirm the results from GSEA, we tested the effect of the combination therapy on the key regulators of the E2F pathway in HSJD-DIPG007 and SU-DIPGVI cells, harboring wild-type TP53 and mutant TP53, respectively. Using western blot analysis and real-time PCR, we showed that the combination therapy markedly reduced the E2F1 pathway at both the protein and RNA levels (Figure 6B; Figures S3A–S3C). We also observed a reduction in phosphorylated Rb, while total Rb protein was not significantly affected. The results also confirmed that the effect of the drugs on the E2F pathway was independent of TP53 status.

We next evaluated the effect of the combination therapy on two upstream regulators of Rb, $p16^{INK4A}$ (*CDKN2A*) and cyclin-

dependent kinase 4 (CDK4). $P16^{INK4A}$ is a CDK inhibitor that induces dephosphorylation of Rb through inhibition of CDK4 (Broude et al., 2007). CBL0137 and panobinostat as single agents had only a modest effect on $p16^{INK4A}$ and CDK4 protein; however, the combination therapy led to a marked increase in $p16^{INK4A}$ and a correlative reduction in CDK4 at both the protein and RNA levels (Figure 6B; Figures S5A–S5C). These results suggest that the effect of combination therapy on the epigenome leads to activation of $p16^{INK4A}$ with consequent inhibition of the E2F pathway. Importantly, the expression of H3.3K27M has been found to recruit epigenetic regulators to repress $p16^{INK4A}$ and that the loss of $p16^{INK4A}$ is central to H3.3K27M-mediated tumor cell proliferation (Cordero et al., 2017), an effect reversed by the combination treatment of CBL0137 and panobinostat.

Given the effects observed on $p16^{INK4A}$ and CDK4, we examined other cell cycle regulators and found that the combination of CBL0137 and panobinostat leads to inhibition of the key regulators of the G_1 to S phase of cell cycle, including MCM2–MCM8, CDK1, cyclin A2, B1, E2F, and WEE1, among others (Figure S4). MCM2–MCM7 proteins form a family of DNA helicases implicated at the initiation of DNA synthesis (Maiorano et al., 2006). The nuclear serine/threonine kinase WEE is a key regulator of cell cycle progression and has been shown to be overexpressed in pediatric gliomas such as DIPG (Duchatel et al., 2019). Approximately 30% of DIPGs are known to have amplification of genes that regulate the G_1 to S cell cycle progression, particularly the cyclin D family members CDK4 and CDK6, as well as reduced levels of p16, an endogenous inhibitor of CDK4/6 (Mohammad et al., 2017; Paugh et al., 2011).

Given the change in H3K27me3 after co-administration of CBL0137 and panobinostat, and that the PRC2 complex genes (EZH2, SUZ12, EED) have been shown to be transcriptionally regulated by the RB/E2F pathway (Bracken et al., 2003), we next sought to determine the effect of combination therapy on EZH2 expression. A significant increase in the methyltransferase activity of the EZH2 was observed following combination therapy with CBL0137 and panobinostat (Figure 6C). Thus, combination treatment with dual epigenetic targeting agents CBL0137 and panobinostat restores $p16^{INK4A}$ activity, inhibits the E2F pathway, increases EZH2 activity, and leads to restoration of H3K27me3.

CBL0137 and panobinostat treatment influences the expression levels of oligodendroglial lineage genes

Recent studies on super-enhancers in DIPG revealed that several dysregulated genes associated with these regions were specifically from an oligodendroglial lineage identity, which contribute to maintaining the malignant state of the disease (Nagaraja et al., 2017). Therefore, we sought to determine whether the combination of CBL0137 and panobinostat preferentially disrupted transcription of oligodendroglial lineage genes using Affymetrix gene expression analysis (Figure S5A). Our results revealed that combination therapy led to downregulation of SOX2 and NES (markers of undifferentiated neural cells), CSPG4, OLIG2, and LINGO1 (associated with oligodendrocyte precursor cells), OLIG1 (expressed by oligodendroglial lineage cells during differentiation), CHD7 and CHD8 (markers of oligodendrocyte precursor survival and differentiation), ASCL1

A

B
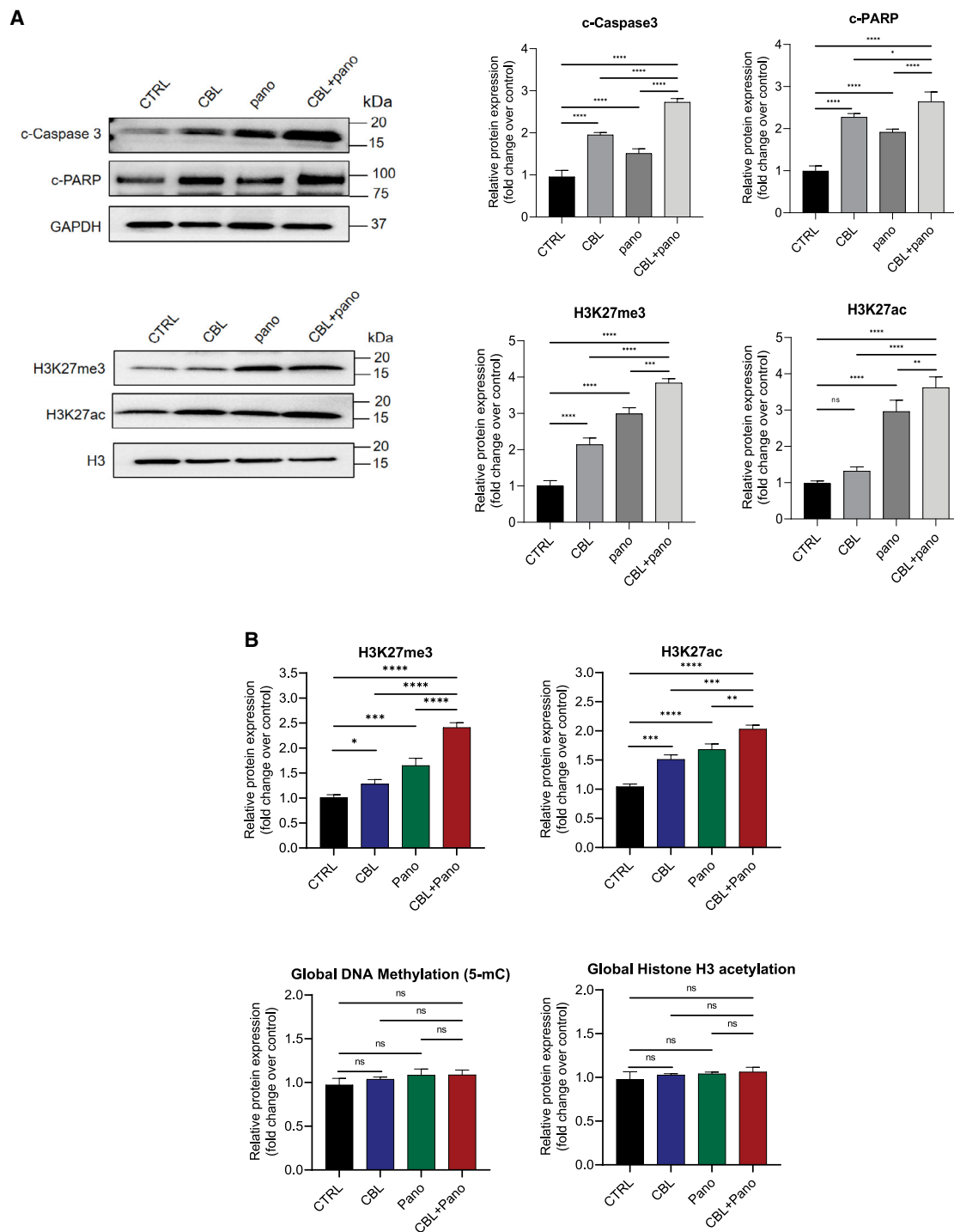
Figure 5. Dual inhibition of FACT and HDAC enhances the expression of apoptotic markers and restores H3K27 trimethylation and acetylation

(A) Combination of CBL0137 (0.6 μM) and panobinostat (20 nM) induces apoptosis (following 48-h treatment) (see also Figure S2B) and increases the protein expression of H3K27me3 and H3K27ac (after 24-h treatment) in HSJD-DIPG007 cells (see also Figure S2B).

(B) An EpiQuik ELISA assay reveals that the effect on the histone marks is specific to H3K27me3 and H3K27ac and that the combination therapy has no effect on the global DNA methylation and histone acetylation (24-h treatment). Data are presented as means ± SD from three independent experiments. A one-way ANOVA with Dunnett's multiple comparison test was used to compare the combination therapy group with single agent treatments. $**p < 0.01$, $***p < 0.001$, $****p < 0.0001$.
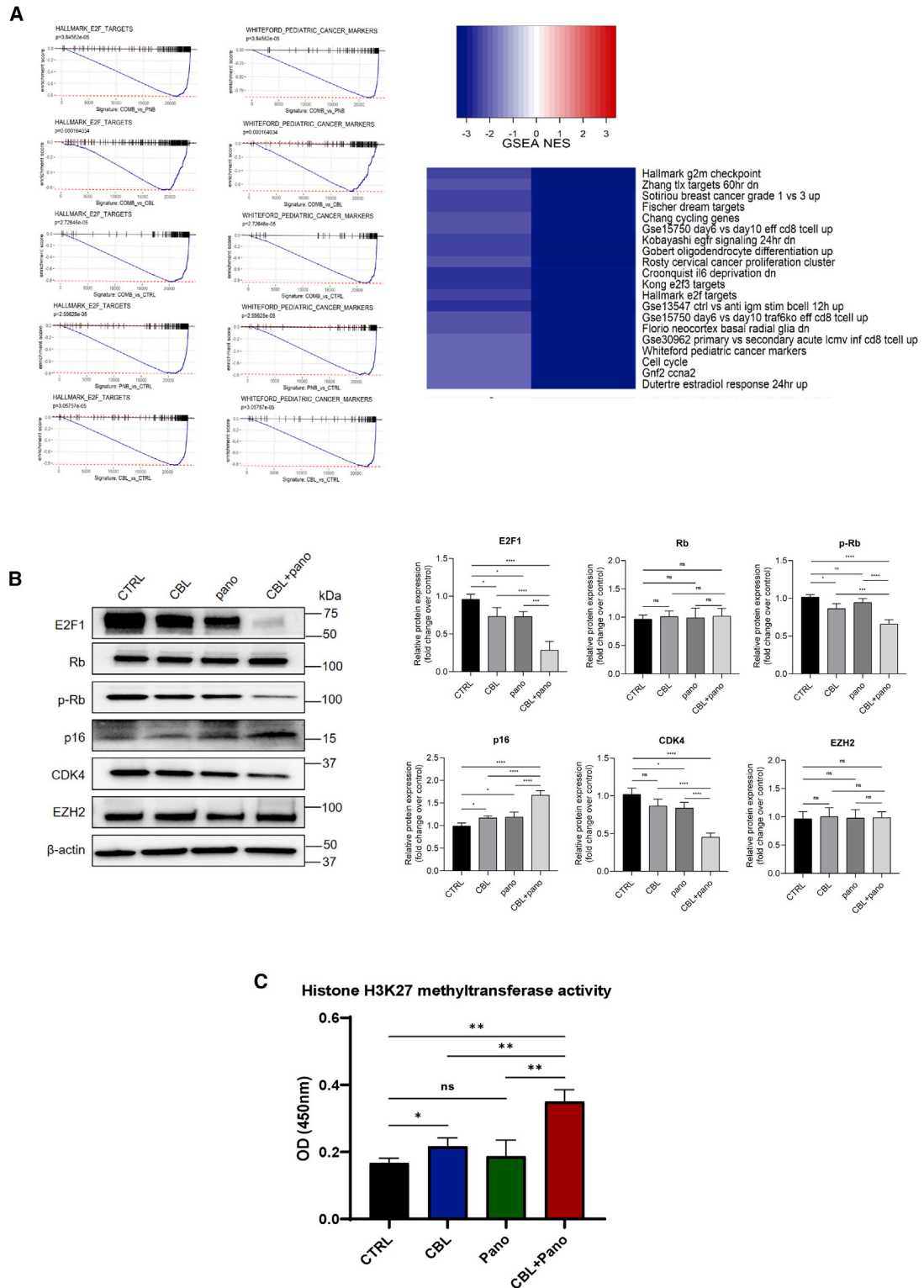
Figure 6. Combination treatment of CBL0137 with panobinostat affects the Rb/E2F pathway and restores the activity of EZH2

(A) Gene set enrichment analysis (GSEA) identified "Whiteford pediatric cancer markers" and "Hallmark E2F targets" as the key pathways affected by the combination of CBL0137 (0.6 μM) and panobinostat (20 nM) in HSJD-DIPG007 cells.

(legend continued on next page)

(promotes neuronal differentiation) (Tang, 2017), as well as CCNB1 and CCND1 (involved in the transition of oligodendrocyte progenitors from proliferation to differentiation mediated by E2F1) (Magri et al., 2014). These results were also confirmed by real-time PCR (Figure S5B).

Combination of CBL0137 and panobinostat significantly extends survival in mice models of DIPG

To further assess the therapeutic potential of CBL0137 and panobinostat, we next investigated the effect of combination therapy in two DIPG orthotopic patient-derived xenograft models. Treatment started at 4 and 9 weeks after inoculation of HSJD-DIPG007 and SU-DUPGVI, respectively. CBL0137 was administered at 40 mg/kg intravenously every 4 days for 4 weeks. Panobinostat was administered intraperitoneally at the dose of 10 mg/kg three times a week for 4 weeks. As shown in Figure 7A, the median survival of vehicle-treated HSJD-DIPG007 orthotopic mice was 77 days. CBL0137 and panobinostat as single agents at these doses did not extend the survival of animals (median survival of 79.5 and 76 days, respectively). However, combination therapy significantly prolonged the survival of animals compared with other treatment groups (median survival = 106 days, p < 0.0001).

For the SU-DIPGVI orthotopic model, CBL0137 was administered at 40 mg/kg intravenously every 4 days for 4 weeks. Panobinostat was administered intraperitoneally at the dose of 5 mg/kg, 5 days on, 2 days off for 4 weeks. The median survival of the vehicle-treated group was 114 days. CBL0137 as a single agent significantly increased the survival of mice (139 days, p = 0.0481 versus control), whereas panobinostat did not have a significant effect on a median survival (138 days, p = 0.580 versus control). However, as seen in the HSJD-DIPG007 model, the combination of the two drugs significantly extended the survival of mice compared with single agents and the vehicle-treated group (median survival = 158, p = 0.0031 versus control), with several mice in the combination group surviving until the endpoint (Figure 7A). Both CBL0137 and panobinostat as single agents and in combination were found to be well tolerated at the doses administered, with no weight loss observed in any group (Figure 7B).

Immunohistochemistry analysis of brain tissues collected 24 h after the final doses of the drugs showed a significant reduction in tumor cell proliferation in the treatment groups, as reflected in the number of positive cells for the proliferation marker Ki-67. Immunohistochemical staining also showed that the combination therapy led to the restoration of H3K27me3 and an increase in H3K27ac in HSJD-DIPG007 xenografted tumors compared with other treatment groups (Figure S6A). CBL0137 treatment also resulted in a significant reduction in SSRP1 and SPT16 levels in tumor cells (Figure S6B). Overall, these results suggest targeting the epigenome with combined inhibition of FACT and HDAC represents a promising therapeutic strategy for DIPG.

DISCUSSION

DIPG represents the most devastating brain tumor of childhood with a median survival of less than a year from diagnosis. Despite more than 250 clinical trials using conventional chemotherapy and targeted therapeutics, no progress has been made to improve this prognosis since the introduction of palliative radiotherapy more than 3 decades ago (Johung and Monje, 2017). Recent comprehensive genomic studies have shown that H3K27M mutations in either histone H3.3 or H3.1 are the hallmark of DIPG pathogenesis. This mutation that is found in 80% of DIPGs leads to the alteration of PRC2 methyltransferase activity, a global hypomethylation of H3K27, and, subsequently, broad epigenomic dysregulation (Lewis et al., 2013).

The histone chaperone FACT influences global chromatin remodeling during DNA transcription, replication, and repair. In this study, we show that FACT is a potential therapeutic target in DIPG. Our results confirmed that pharmacologic inhibition of FACT by CBL0137 treatment suppressed the proliferation of DIPG cells. This decrease in proliferation was directly comparable to that observed from the knockdown of the two FACT subunits SSRP1 and SPT16. Importantly, we identified a direct interaction between SSRP1 and H3K27M, suggesting that targeting FACT offers a strategy for inhibiting this critical epigenetic driver, thus changing the mutational profile that defines DIPG, and reverting the epigenetic signature of mutated H3K27. The FACT complex is known to maintain nucleosome integrity through the interactions of SSRP1 with H3/H4 tetramers during DNA replication and transcription (Chen et al., 2018). Furthermore, SSRP1 has also been reported to be enriched together with wild-type H3.3 in specific locations that required increased transcription and rapid histone turnover, leading to somatic hypermutation in Burkitt's lymphoma cells (Aida et al., 2013). Further studies are needed to elucidate the precise relationship between H3K27M and the FACT complex and whether the FACT complex colocalizes at same genomic regions as H3K27M in DIPG. Previous studies revealed that CBL0137 inhibits proliferation of cancer cells by destabilizing chromatin and activating the p53 pathway through chromatin trapping of FACT in glioblastoma cells (Gasparian et al., 2011). Our data from microarray analyses showed that cell cycle and p53 signaling pathways are the most enriched pathways in KEGG pathway enrichment analysis. Interestingly, however, our results reveal that the antiproliferative effect of CBL0137 was independent of p53 status of the cells, consistent with previous studies of CBL0137 on neuroblastoma and adult cancers (Carter et al., 2015; Gasparian et al., 2011).

Given the aggressive nature of DIPG, and its inherent resistance to anti-cancer agents, it is increasingly accepted that combinatorial approaches are essential to improve patient outcomes. Also, efficient drug delivery to DIPG tumors is one of the major challenges that contribute to limited treatment options

---

(B) Key regulators of the Rb/E2F pathway are affected by the combination of CBL0137 and panobinostat (see also Figures S5A–S5C).

(C) Combination of CBL0137 and panobinostat increases the enzymatic activity of EZH2 compared with single-agent treatments.

Data are presented as means ± SD of at least three independent experiments. Densitometry analysis was performed using ImageJ software from at least four independent experiments. A one-way ANOVA with Dunnett's multiple comparison test was used to compare mean of the combination therapy group with single-agent treatments. *p < 0.05, **p < 0.01, ***p < 0.001, ****p < 0.0001.

A

B
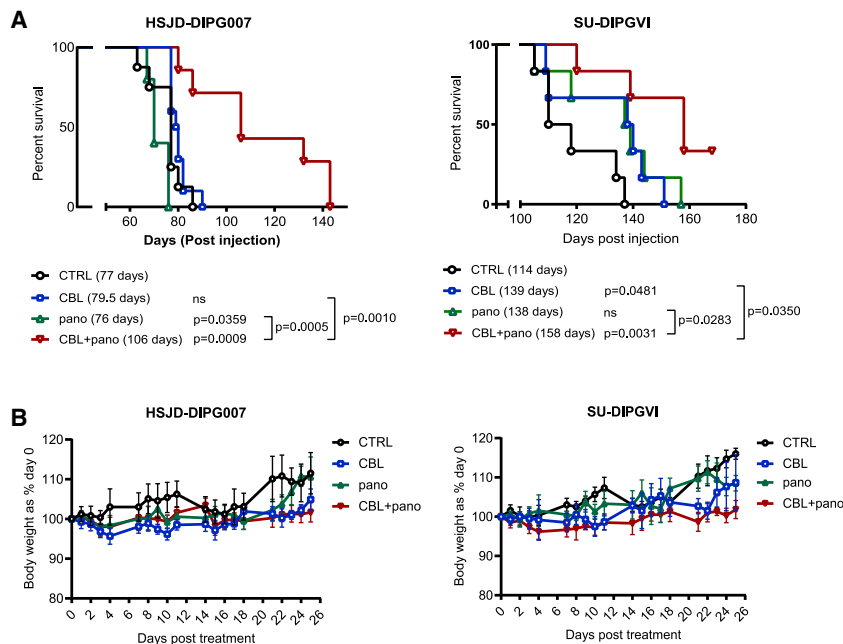
Figure 7. Combination of CBL0137 with panobinostat extends survival in the orthotopic patient-derived mouse models of DIPG

(A) Combination of CBL0137 and panobinostat significantly extends survival in the mouse models of HSJD-DIPG007 (left panel) and SU-DIPGVI (right panel) cells. In the HSJD-DIPG007 model, mice were implanted with HSJD-DIPG007 cells intracranially. After 4 weeks, the animals were treated with vehicle, CBL0137 (40 mg/kg; i.v.; every 4 days for 4 weeks), panobinostat (10 mg/kg; intraperitoneally [i.p.]; Monday, Wednesday, and Friday for 4 weeks), or the combination of the two agents. For the SU-DIPGVI model, BALB/c nude mice were intracranially injected with cells. After 9 weeks, the animals were treated with vehicle, CBL0137 (40 mg/kg; i.v.; every 4 days for 4 weeks), panobinostat (5 mg/kg; i.p.; 5 days on, 2 days off for 4 weeks), or the combination of the two agents (see also Figure S6).

(B) Tolerability of NOD/SCID and BALB/c nude mice exposed to different doses/schedules of CBL0137, panobinostat, and their combination as evaluated by body weight relative to day 0. A log-rank (Mantel-Cox) test was used to determine statistical significance between treatment groups.

for patients (Vanan and Eisenstat, 2015). In the present study, we confirmed that CBL0137 efficiently crosses the BBB. We found that the brain concentrations of CBL0137 were more than 50-fold higher than that in the plasma, boding well for clinical translation. Furthermore, we showed that FACT inhibition by CBL0137 exhibits a therapeutic synergy with the HDACi panobinostat, which has shown activity in preclinical models of DIPG (Grasso et al., 2015; Hennika et al., 2017). Panobinostat also exhibited a disease-specific mechanism, restoring H3K27me3 and normalizing oncogenic gene expression (Grasso et al., 2015). We found that the combination of CBL0137 and panobinostat increased both H3K27ac and H3K27me3 levels and synergistically induced apoptosis. Importantly, despite the activity of panobinostat in preclinical models, these results to date have not been translated to the clinic. Clinical trials to date have shown that panobinostat could not be escalated to sufficiently high doses to have single-agent activity in DIPG patients (Cooney et al., 2018). The combined epigenetically targeted therapy in this study offers the potential to enhance the activity of panobinostat at dose levels that are achievable clinically. Notably, the dose of panobinostat used in the in vivo model, while well tolerated, had no single agent activity, while the combination treatment at the same dosage had a potent impact on survival.

Importantly, we found through Affymetrix gene expression analysis that CBL0137 and panobinostat synergistically disrupt the Rb/E2F1 pathway. Subsequent experiments confirmed that this effect is primarily through upstream regulators of Rb, tumor suppressor p16[INK4A] (CDKN2A), and CDK4. The p16[INK4a]-Cdk4-Rb axis critically regulates G_1 to S phase progression where p16[INK4A] downregulates CDK4, thereby dephosphorylating Rb. Hypophosphorylated Rb interacts with E2F1, resulting in repression of the cell cycle and proliferation arrest. Dysregulation of the Rb pathway is common in pediatric brain cancers (Diaz and Baker, 2014). Similarly, 30% of DIPGs are known to have ampli-

fication of genes that regulate G_1 to S cell cycle progression, particularly the cyclin D family members CDK4 and CDK6 (Mohammad et al., 2017; Paugh et al., 2011). In contrast, CDKN2A deletion, although it is frequently seen in adults with high-grade gliomas (HGGs) (>55%) (Brennan et al., 2013), is rarely reported in pediatric high-grade gliomas (Mackay et al., 2017). Nevertheless, it has been recently demonstrated that p16[INK4A] is a direct target of H3.3K27M and that CDKN2A knockout abolishes the difference in survival between H3.3K27M and H3.3WT tumors in a murine model of DIPG (Cordero et al., 2017). This highlights that p16[INK4A] rescue through regulation of CDK4 and the G_1 to S transition may be an important tumorigenic mechanism in DIPG.

Affymetrix analyses also revealed that treatment with CBL0137 and panobinostat disrupted transcription of a number of genes from oligodendroglial lineage identity that are associated with super-enhancers in DIPG and represent the DIPG cell of origin and maintain the malignant state of DIPG (Marie et al., 2018; Monje et al., 2011; Nagaraja et al., 2017). These include markers of undifferentiated neural cells (SOX2 and NES), genes associated with oligodendrocyte precursor cells (CSPG4 or NG2, OLIG2, LINGO1), a gene expressed by oligodendroglial lineage cells during differentiation (OLIG1), the marker of neuronal differentiation (ASCL1) (Tang, 2017), and, finally, the markers of oligodendrocyte precursor survival and differentiation (chd7, chd8) (Marie et al., 2018; Monje et al., 2011; Nagaraja et al., 2017). It has been suggested that targeting the genes involved in neurogenesis and development of the nervous system may provide a novel avenue for targeted therapy development to impair the proliferation of DIPG (Azzarelli et al., 2018). For instance, a recent study revealed that neuronal activity-regulated secretion of the synaptic protein neuroligin-3 (NG3) increased the proliferation of DIPG cells through induction of the phosphatidylinositol 3-kinase (PI3K)-mTOR pathway and that the expression of NG3 inversely correlated with survival in

patients with high-grade gliomas (Venkatesh et al., 2015). Another study suggested that neuron-glial antigen 2 (NG2 or CSPG4) expression is prominent in most DIPG cohort samples as well as preclinical models of DIPG, and that orthotopic injection of NG2-expressing cells resulted in rapidly developing pontine tumors (Yadavilli et al., 2015). Nevertheless, "differentiation therapy" is still an unexplored avenue in DIPG, and future studies are needed for better understanding the dysregulated developmental phenotype in DIPG as well as potential future pharmacological development.

Given that H3K27me3 is catalyzed by EZH2 methyltransferase activity, and that the PRC2 complex is regulated by the E2F pathway, we also evaluated the effect of combination therapy on EZH2. We did not observe any changes in either the protein level or gene expression of EZH2. This finding is in line with previous studies, showing that H3K27M mutation is sufficient to reduce H3K27me3 (Lewis et al., 2013) and that this reduction occurs in the absence of EZH2 alteration (Chan et al., 2013; Johung and Monje, 2017; Venneti et al., 2013). However, we found that the combination of CBL0137 and panobinostat increases its histone methyltransferase activity, suggesting that the observed increase in H3K27me3 could be at least in part due to the restoration of histone methyltransferase activity of EZH2. Previous studies have shown that EZH2 undergoes several post-translational modifications that regulate EZH2 activity (Gan et al., 2018) and that phosphorylation of EZH2 at various sites results in the suppression of its enzymatic activity (Chen et al., 2010). Taken together, we have shown that combined epigenetic therapy can regulate EZH2 function to restore the methylation required for a quiescent epigenome.

In summary, the data presented herein demonstrate that FACT inhibition represents a promising therapeutic strategy for DIPG and potently enhances the epigenetic modifying effect of HDAC inhibition. We showed that CBL0137 synergizes with panobinostat to restore p16INK4A activity, inhibit the E2F pathway, and increase EZH2 activity with restoration of H3K27me3. This leads to a potent synergistic effect both *in vitro* and *in vivo*. Panobinostat is clinically available with established pediatric dosing. CBL0137 has just completed phase 1 testing in the adult population and was well tolerated, with minimal toxicity, and is ready for testing in the pediatric setting. Our preclinical data suggest that dual inhibition of the FACT complex and HDAC may represent a promising therapeutic avenue, warranting clinical investigation in children with DIPG.

STAR★METHODS

Detailed methods are provided in the online version of this paper and include the following:

- KEY RESOURCES TABLE
- RESOURCE AVAILABILITY
  - Lead contact
  - Materials availability
  - Data and code availability
- EXPERIMENTAL MODEL AND SUBJECT DETAILS
  - Cell culture models
  - Animal models

- METHOD DETAILS
  - High-throughput drug screening and cell viability assays
  - Clonogenic assay
  - Western blot analysis
  - Apoptosis assay
  - shRNA-expressing lentivirus preparation
  - Co-immunoprecipitation assay
  - Enzyme-linked immunosorbent assay (ELISA)
  - RT² Profiler PCR array and real-time PCR
  - Affymetrix gene expression analysis
  - Immunohistochemistry
  - *In vivo* drug treatment
  - LC-MS/MS determination of CBL0137 concentration in blood and tissue samples
- QUANTIFICATION AND STATISTICAL ANALYSIS

AUTHOR CONTRIBUTIONS

M.H., M.D.N., and D.S.Z. conceived the project. A.V.G and K.G. advised and provided materials for the project. A.E. designed the research study. A.E., S.S., J.L., E.H., A. Khan, R.L., A. Kankean, and M.T. performed *in vitro* experiments. A.E., S.J., C.U., A.G., O.T., M.T., and P.T. conducted *in vivo* experiments. F.M.G., C.N.I.P., and C.M. performed the Affymetrix gene expression analysis. J.R.C.R. and O.V. performed the co-immunoprecipitation assays. R.P. performed pharmacokinetic analysis. M.T., L.F., O.V., Y.T., K.G., and S.S. provided important insights on experiments. A.E. wrote the manuscript. D.S.Z., M.T., L.F., O.V., and M.D.N. revised the manuscript. D.S.Z. supervised the project. All authors reviewed the manuscript.

REFERENCES

Aida, M., Hamad, N., Stanlie, A., Begum, N.A., and Honjo, T. (2013). Accumulation of the FACT complex, as well as histone H3.3, serves as a target marker for somatic hypermutation. Proc. Natl. Acad. Sci. USA *110*, 7784–7789.

Azzarelli, R., Simons, B.D., and Philpott, A. (2018). The developmental origin of brain tumours: A cellular and molecular framework. Development *145*, dev162693.

Barone, T.A., Burkhart, C.A., Safina, A., Haderski, G., Gurova, K.V., Purmal, A.A., Gudkov, A.V., and Plunkett, R.J. (2017). Anticancer drug candidate CBL0137, which inhibits histone chaperone FACT, is efficacious in preclinical orthotopic models of temozolomide-responsive and -resistant glioblastoma. Neuro-oncol. *19*, 186–196.

Bracken, A.P., Pasini, D., Capra, M., Prosperini, E., Colli, E., and Helin, K. (2003). *EZH2* is downstream of the pRB-E2F pathway, essential for proliferation and amplified in cancer. EMBO J. *22*, 5323–5335.

Brennan, C.W., Verhaak, R.G., McKenna, A., Campos, B., Noushmehr, H., Salama, S.R., Zheng, S., Chakravarty, D., Sanborn, J.Z., Berman, S.H., et al.; TCGA Research Network (2013). The somatic genomic landscape of glioblastoma. Cell *155*, 462–477.

Broude, E.V., Swift, M.E., Vivo, C., Chang, B.D., Davis, B.M., Kalurupalle, S., Blagosklonny, M.V., and Roninson, I.B. (2007). p21$^{Waf1/Cip1/Sdi1}$ mediates retinoblastoma protein degradation. Oncogene *26*, 6954–6958.

Brown, Z.Z., Müller, M.M., Jain, S.U., Allis, C.D., Lewis, P.W., and Muir, T.W. (2014). Strategy for "detoxification" of a cancer-derived histone mutant based on mapping its interaction with the methyltransferase PRC2. J. Am. Chem. Soc. *136*, 13498–13501.

Burgess, R.J., and Zhang, Z. (2013). Histone chaperones in nucleosome assembly and human disease. Nat. Struct. Mol. Biol. *20*, 14–22.

Burkhart, C., Fleyshman, D., Kohrn, R., Commane, M., Garrigan, J., Kurbatov, V., Toshkov, I., Ramachandran, R., Martello, L., and Gurova, K.V. (2014). Curaxin CBL0137 eradicates drug resistant cancer stem cells and potentiates efficacy of gemcitabine in preclinical models of pancreatic cancer. Oncotarget *5*, 11038–11053.

Carter, D.R., Murray, J., Cheung, B.B., Gamble, L., Koach, J., Tsang, J., Sutton, S., Kalla, H., Syed, S., Gifford, A.J., et al. (2015). Therapeutic targeting of the MYC signal by inhibition of histone chaperone FACT in neuroblastoma. Sci. Transl. Med. *7*, 312ra176.

Chan, K.M., Fang, D., Gan, H., Hashizume, R., Yu, C., Schroeder, M., Gupta, N., Mueller, S., James, C.D., Jenkins, R., et al. (2013). The histone H3.3K27M mutation in pediatric glioma reprograms H3K27 methylation and gene expression. Genes Dev. *27*, 985–990.

Chen, S., Bohrer, L.R., Rai, A.N., Pan, Y., Gan, L., Zhou, X., Bagchi, A., Simon, J.A., and Huang, H. (2010). Cyclin-dependent kinases regulate epigenetic gene silencing through phosphorylation of EZH2. Nat. Cell Biol. *12*, 1108–1114.

Chen, P., Dong, L., Hu, M., Wang, Y.Z., Xiao, X., Zhao, Z., Yan, J., Wang, P.Y., Reinberg, D., Li, M., et al. (2018). Functions of FACT in breaking the nucleosome and maintaining its integrity at the single-nucleosome level. Mol. Cell *71*, 284–293.e4.

Cooney, T., Lane, A., Bartels, U., Bouffet, E., Goldman, S., Leary, S.E.S., Foreman, N.K., Packer, R.J., Broniscer, A., Minturn, J.E., et al. (2017). Contemporary survival endpoints: An International Diffuse Intrinsic Pontine Glioma Registry study. Neuro-oncol. *19*, 1279–1280.

Cooney, T., Onar-Thomas, A., Huang, J., Lulla, R., Fangusaro, J., Kramer, K., Baxter, P., Fouladi, M., Dunkel, I.J., Warren, K.E., and Monje, M. (2018). DIPG-22. A phase 1 trial of the histone deacetylase inhibitor panobinostat in pediatric patients with recurrent or refractory diffuse intrinsic pontine glioma: A Pediatric Brain Tumor Consortium (PBTC) study. Neuro-oncol. *20* (*Suppl 2*), i53.

Cordero, F.J., Huang, Z., Grenier, C., He, X., Hu, G., McLendon, R.E., Murphy, S.K., Hashizume, R., and Becher, O.J. (2017). Histone H3.3K27M represses *p16* to accelerate gliomagenesis in a murine model of DIPG. Mol. Cancer Res. *15*, 1243–1254.

Dermawan, J.K., Gurova, K., Pink, J., Dowlati, A., De, S., Narla, G., Sharma, N., and Stark, G.R. (2014). Quinacrine overcomes resistance to erlotinib by inhibiting FACT, NF-κB, and cell-cycle progression in non-small cell lung cancer. Mol. Cancer Ther. *13*, 2203–2214.

Diaz, A.K., and Baker, S.J. (2014). The genetic signatures of pediatric high-grade glioma: No longer a one-act play. Semin. Radiat. Oncol. *24*, 240–247.

Duchatel, R.J., Jackson, E.R., Alvaro, F., Nixon, B., Hondermarck, H., and Dun, M.D. (2019). Signal transduction in diffuse intrinsic pontine glioma. Proteomics *19*, e1800479.

Gan, L., Yang, Y., Li, Q., Feng, Y., Liu, T., and Guo, W. (2018). Epigenetic regulation of cancer progression by EZH2: From biological insights to therapeutic potential. Biomark. Res. *6*, 10.

Garcia, H., Fleyshman, D., Kolesnikova, K., Safina, A., Commane, M., Paszkiewicz, G., Omelian, A., Morrison, C., and Gurova, K. (2011). Expression of FACT in mammalian tissues suggests its role in maintaining of undifferentiated state of cells. Oncotarget *2*, 783–796.

Garcia, H., Miecznikowski, J.C., Safina, A., Commane, M., Ruusulehto, A., Kilpinen, S., Leach, R.W., Attwood, K., Li, Y., Degan, S., et al. (2013). Facilitates chromatin transcription complex is an "accelerator" of tumor transformation and potential marker and target of aggressive cancers. Cell Rep. *4*, 159–173.

Gasparian, A.V., Burkhart, C.A., Purmal, A.A., Brodsky, L., Pal, M., Saranadasa, M., Bosykh, D.A., Commane, M., Guryanova, O.A., Pal, S., et al. (2011). Curaxins: Anticancer compounds that simultaneously suppress NF-κB and activate p53 by targeting FACT. Sci. Transl. Med. *3*, 95ra74.

Grasso, C.S., Tang, Y., Truffaux, N., Berlow, N.E., Liu, L., Debily, M.A., Quist, M.J., Davis, L.E., Huang, E.C., Woo, P.J., et al. (2015). Functionally defined therapeutic targets in diffuse intrinsic pontine glioma. Nat. Med. *21*, 827.

Grill, J., Puget, S., Andreiuolo, F., Philippe, C., MacConaill, L., and Kieran, M.W. (2012). Critical oncogenic mutations in newly diagnosed pediatric diffuse intrinsic pontine glioma. Pediatr Blood Cancer *58*, 489–491.

Harbour, J.W., and Dean, D.C. (2000). The Rb/E2F pathway: Expanding roles and emerging paradigms. Genes Dev. *14*, 2393–2409.

Hashizume, R. (2017). Epigenetic targeted therapy for diffuse intrinsic pontine glioma. Neurol. Med. Chir. (Tokyo) *57*, 331–342.

Hennika, T., Hu, G., Olaciregui, N.G., Barton, K.L., Ehteda, A., Chitranjan, A., Chang, C., Gifford, A.J., Tsoli, M., Ziegler, D.S., et al. (2017). Pre-clinical study of panobinostat in xenograft and genetically engineered murine diffuse intrinsic pontine glioma models. PLoS ONE *12*, e0169485.

Johung, T.B., and Monje, M. (2017). Diffuse intrinsic pontine glioma: new pathophysiological insights and emerging therapeutic targets. Curr. Neuropharmacol. *15*, 88–97.

Koman, I.E., Commane, M., Paszkiewicz, G., Hoonjan, B., Pal, S., Safina, A., Toshkov, I., Purmal, A.A., Wang, D., Liu, S., et al. (2012). Targeting FACT complex suppresses mammary tumorigenesis in *Her2/neu* transgenic mice. Cancer Prev. Res. (Phila.) *5*, 1025–1035.

Lewis, P.W., Müller, M.M., Koletsky, M.S., Cordero, F., Lin, S., Banaszynski, L.A., Garcia, B.A., Muir, T.W., Becher, O.J., and Allis, C.D. (2013). Inhibition of PRC2 activity by a gain-of-function H3 mutation found in pediatric glioblastoma. Science *340*, 857–861.

Mackay, A., Burford, A., Carvalho, D., Izquierdo, E., Fazal-Salom, J., Taylor, K.R., Bjerke, L., Clarke, M., Vinci, M., Nandhabalan, M., et al. (2017). Integrated molecular meta-analysis of 1,000 pediatric high-grade and diffuse intrinsic pontine glioma. Cancer Cell *32*, 520–537.e5.

Magri, L., Swiss, V.A., Jablonska, B., Lei, L., Pedre, X., Walsh, M., Zhang, W., Gallo, V., Canoll, P., and Casaccia, P. (2014). E2F1 coregulates cell cycle genes and chromatin components during the transition of oligodendrocyte progenitors from proliferation to differentiation. J. Neurosci. *34*, 1481–1493.

Maiorano, D., Lutzmann, M., and Méchali, M. (2006). MCM proteins and DNA replication. Curr. Opin. Cell Biol. *18*, 130–136.

Marie, C., Clavairoly, A., Frah, M., Hmidan, H., Yan, J., Zhao, C., Van Steenwinckel, J., Daveau, R., Zalc, B., Hassan, B., et al. (2018). Oligodendrocyte precursor survival and differentiation requires chromatin remodeling by Chd7 and Chd8. Proc. Natl. Acad. Sci. USA *115*, E8246–E8255.

Mohammad, F., Weissmann, S., Leblanc, B., Pandey, D.P., Højfeldt, J.W., Comet, I., Zheng, C., Johansen, J.V., Rapin, N., Porse, B.T., et al. (2017). EZH2 is a potential therapeutic target for H3K27M-mutant pediatric gliomas. Nat. Med. 23, 483–492.

Molania, R., Gagnon-Bartsch, J.A., Dobrovic, A., and Speed, T.P. (2019). A new normalization for Nanostring nCounter gene expression data. Nucleic Acids Res. 47, 6073–6083.

Monje, M., Mitra, S.S., Freret, M.E., Raveh, T.B., Kim, J., Masek, M., Attema, J.L., Li, G., Haddix, T., Edwards, M.S., et al. (2011). Hedgehog-responsive candidate cell of origin for diffuse intrinsic pontine glioma. Proc. Natl. Acad. Sci. USA 108, 4453–4458.

Mylonas, C., and Tessarz, P. (2018). Transcriptional repression by FACT is linked to regulation of chromatin accessibility at the promoter of ES cells. Life Sci. Alliance 1, e201800085.

Nagaraja, S., Vitanza, N.A., Woo, P.J., Taylor, K.R., Liu, F., Zhang, L., Li, M., Meng, W., Ponnuswami, A., Sun, W., et al. (2017). Transcriptional dependencies in diffuse intrinsic pontine glioma. Cancer Cell 31, 635–652.e6.

Nevins, J.R. (2001). The Rb/E2F pathway and cancer. Hum. Mol. Genet. 10, 699–703.

Neznanov, N., Gorbachev, A.V., Neznanova, L., Komarov, A.P., Gurova, K.V., Gasparian, A.V., Banerjee, A.K., Almasan, A., Fairchild, R.L., and Gudkov, A.V. (2009). Anti-malaria drug blocks proteotoxic stress response: anti-cancer implications. Cell Cycle 8, 3960–3970.

Paugh, B.S., Broniscer, A., Qu, C., Miller, C.P., Zhang, J., Tatevossian, R.G., Olson, J.M., Geyer, J.R., Chi, S.N., da Silva, N.S., et al. (2011). Genome-wide analyses identify recurrent amplifications of receptor tyrosine kinases and cell-cycle regulatory genes in diffuse intrinsic pontine glioma. J. Clin. Oncol. 29, 3999–4006.

Piunti, A., Hashizume, R., Morgan, M.A., Bartom, E.T., Horbinski, C.M., Marshall, S.A., Rendleman, E.J., Ma, Q., Takahashi, Y.H., Woodfin, A.R., et al. (2017). Therapeutic targeting of polycomb and BET bromodomain proteins in diffuse intrinsic pontine gliomas. Nat. Med. 23, 493–500.

Preet, R., Mohapatra, P., Mohanty, S., Sahu, S.K., Choudhuri, T., Wyatt, M.D., and Kundu, C.N. (2012). Quinacrine has anticancer activity in breast cancer cells through inhibition of topoisomerase activity. Int. J. Cancer 130, 1660–1670.

Ritchie, M.E., Phipson, B., Wu, D., Hu, Y., Law, C.W., Shi, W., and Smyth, G.K. (2015). limma powers differential expression analyses for RNA-sequencing and microarray studies. Nucleic Acids Res. 43, e47.

Schroeder, K.M., Hoeman, C.M., and Becher, O.J. (2014). Children are not just little adults: Recent advances in understanding of diffuse intrinsic pontine glioma biology. Pediatr. Res. 75, 205–209.

Schwartzentruber, J., Korshunov, A., Liu, X.Y., Jones, D.T., Pfaff, E., Jacob, K., Sturm, D., Fontebasso, A.M., Quang, D.A., Tönjes, M., et al. (2012). Driver mutations in histone H3.3 and chromatin remodelling genes in paediatric glioblastoma. Nature 482, 226–231.

Sturm, D., Witt, H., Hovestadt, V., Khuong-Quang, D.A., Jones, D.T., Konermann, C., Pfaff, E., Tönjes, M., Sill, M., Bender, S., et al. (2012). Hotspot mutations in H3F3A and IDH1 define distinct epigenetic and biological subgroups of glioblastoma. Cancer Cell 22, 425–437.

Tang, B.L. (2017). The potential of targeting brain pathology with Ascl1/Mash1. Cells 6, 26.

Tsoli, M., Liu, J., Franshaw, L., Shen, H., Cheng, C., Jung, M., Joshi, S., Ehteda, A., Khan, A., Montero-Carcabosso, A., et al. (2018). Dual targeting of mitochondrial function and mTOR pathway as a therapeutic strategy for diffuse intrinsic pontine glioma. Oncotarget 9, 7541–7556.

Vanan, M.I., and Eisenstat, D.D. (2015). DIPG in Children - What Can We Learn from the Past? Front Oncol 5, 237.

Venkatesh, H.S., Johung, T.B., Caretti, V., Noll, A., Tang, Y., Nagaraja, S., Gibson, E.M., Mount, C.W., Polepalli, J., Mitra, S.S., et al. (2015). Neuronal activity promotes glioma growth through neuroligin-3 secretion. Cell 161, 803–816.

Venneti, S., Garimella, M.T., Sullivan, L.M., Martinez, D., Huse, J.T., Heguy, A., Santi, M., Thompson, C.B., and Judkins, A.R. (2013). Evaluation of histone 3 lysine 27 trimethylation (H3K27me3) and enhancer of Zest 2 (EZH2) in pediatric glial and glioneuronal tumors shows decreased H3K27me3 in H3F3A K27M mutant glioblastomas. Brain Pathol. 23, 558–564.

Wu, G., Broniscer, A., McEachron, T.A., Lu, C., Paugh, B.S., Becksfort, J., Qu, C., Ding, L., Huether, R., Parker, M., et al.; St. Jude Children's Research Hospital–Washington University Pediatric Cancer Genome Project (2012). Somatic histone H3 alterations in pediatric diffuse intrinsic pontine gliomas and non-brainstem glioblastomas. Nat. Genet. 44, 251–253.

Yadavilli, S., Scafidi, J., Becher, O.J., Saratsis, A.M., Hiner, R.L., Kambhampati, M., Mariarita, S., MacDonald, T.J., Codispoti, K.E., Magge, S.N., et al. (2015). The emerging role of NG2 in pediatric diffuse intrinsic pontine glioma. Oncotarget 6, 12141–12155.

STAR★METHODS

KEY RESOURCES TABLE

REAGENT or RESOURCE	SOURCE	IDENTIFIER
Antibodies		
Rabbit monoclonal anti-Ezh2 (D2C9)	Cell Signaling Technology	Cat# 5246; RRID: AB_10694683
Rabbit monoclonal anti-SPT16 (D7I2K)	Cell Signaling Technology	Cat# 12191; RRID: AB_2732025
Rabbit monoclonal anti-SSRP1 (E1Y8D)	Cell Signaling Technology	Cat# 13421; RRID: AB_2714160
Rabbit monoclonal anti-p16 INK4A (D7C1M)	Cell Signaling Technology	Cat# 80772; RRID: AB_2799960
Rabbit monoclonal anti- E2F-1	Cell Signaling Technology	Cat# 3742; RRID: AB_2096936
Rabbit monoclonal anti-Rb (D20)	Cell Signaling Technology	Cat# 9313; RRID: AB_1904119
Rabbit monoclonal anti-Phospho-Rb (Ser807/811) (D20B12)	Cell Signaling Technology	Cat# 8516; RRID: AB_11178658
Rabbit monoclonal anti-GAPDH (14C10)	Cell Signaling Technology	Cat# 2118; RRID: AB_561053
Rabbit monoclonal anti-β-Actin (D6A8)	Cell Signaling Technology	Cat# 8457; RRID: AB_10950489
Rabbit monoclonal anti-CDK4 (D9G3E)	Cell Signaling Technology	Cat# 12790; RRID: AB_2631166
Rabbit poyclonal anti-SSRP1	Origene	Cat# TA308461
Mouse monoclonal anti-SUPT16H [Clone ID: OTI8A1]	Thermo Fisher Scientific	Cat# MA5-27214; RRID: AB_2723679
Rabbit monoclonal anti- Ki67 [EPR3610]	Abcam	Cat# ab209897; RRID: AB_2756822
Rabbit monoclonal anti-Histone H3 (acetyl K27) antibody [EP16602]	Abcam	Cat# ab177178; RRID: AB_2828007
Rabbit monoclonal anti-Histone H3 (tri methyl K27) antibody (ab6002)	Abcam	Cat# ab6002; RRID: AB_305237
Rabbit monoclonal anti-gamma H2A.X (phospho S139)	Abcam	Cat# ab26350; RRID: AB_470861
Rabbit monoclonal anti-Cleaved Caspase-3 (Asp175) (5A1E)	Cell Signaling Technology	Cat# 9664; RRID: AB_2070042
Rabbit monoclonal anti-Cleaved PARP (Asp214) (D64E10)	Cell Signaling Technology	Cat# 5625; RRID: AB_10699459
Rabbit monoclonal anti-Histone H3 (3H1)	Cell Signaling Technology	Cat# 9717; RRID: AB_331222
Rabbit monoclonal anti-Tri-Methyl-Histone H3 (Lys27) (C36B11	Cell Signaling Technology	Cat# 9733; RRID: AB_2616029
Rabbit monoclonal anti-Acetyl-Histone H3 (Lys27) (D5E4)	Cell Signaling Technology	Cat# 8173; RRID: AB_10949503
Rabbit monoclonal anti- Histone H3 (K27M Mutant Specific) (D3B5T)	Cell Signaling Technology	Cat# 74829; RRID: AB_2799861
Rabbit IgG Isotype Control antibody	Thermo Fisher Scientific	Cat# 10500C; RRID: AB_2532981
H3K27ac Polyclonal Antibody	Thermo Fisher Scientific	Cat# MA5-31760; RRID: AB_2787383
SSRP1 Polyclonal Antibody	Thermo Fisher Scientific	Cat# PA5-22186; RRID: AB_11152162
SUPT16H Monoclonal Antibody	Thermo Fisher Scientific	Cat# MA5-27214; RRID: AB_2723679
Biological samples		
Patient-derived xenografts (PDX) SU-DIPGs (VI and XVII) and HSJD-DIPGs (007, 011, 012, 013) VUMC-DIPG10	Stanford University (USA) and St John of Hope Hospital (Spain)	A/Prof Michelle Monje and Dr Angel Montero Carcaboso Prof Esther Hulleman
Chemicals, peptides, and recombinant proteins		
SeaPlaqueTM GTGTM Agarose	LONZA	Catalog #: 50115
CBL0137	Incuron, Inc	https://incuron.com/
Panobinostat	Selleckchem	Cat # S1030; Cas# 404950-80-7
Critical commercial assays		
ViraPower Lentiviral Packaging	Thermo Fisher Scientific	Cat# K497500
Histone H3 (K27) Methyltransferase Activity Quantification Assay Kit	Abcam	Cat# ab113454
RNeasy 96 Kit	QIAGEN	Cat # 74181
RT2 First Strand Kit	QIAGEN	Cat # 330401

(Continued on next page)

Continued

REAGENT or RESOURCE	SOURCE	IDENTIFIER
RT^2 Profiler PCR Array Human Cell Cycle	QIAGEN	Cat# PAHS-020Z; product# 330231
RT^2 Profiler PCR Array Human Polycomb	QIAGEN	Cat# PAHS-505Z; product# 330231
Histone Extraction Kit	Abcam	Cat# ab113476
Genomic DNA Extraction Kit	Abcam	Cat# ab156900
EpiQuik Global Acetyl Histone H3K27 Quantification Kit	Epigentek	Cat # P-4059
EpiQuik Global Histone H3 Acetylation Assay Kit	Epigentek	Cat # P-4008
EpiQuik Global Tri-Methyl Histone H3K27 Quantification Kit	Epigentek	Cat # P-3042
MethylFlash Methylated DNA 5-mC Quantification Kit	Epigentek	Cat # P-1034
Deposited data		
Raw and analyzed data	This paper	N/A
Affymetrxi gene expression analysis; Effect of the combination of CBL0137 and Panobinostat on HSJD-DIPG007 cells	This paper	https://www.ncbi.nlm.nih.gov/geo/query.acc.cgi?acc=GSE153441
Affymetrxi gene expression analysis; Effect of CBL0137 on HSJD-DIPG007 cells	This paper	https://www.ncbi.nlm.nih.gov/geo/query.acc.cgi?acc=GSE153883
Oligonucleotides		
Primers for RT-qPCR	Origene	Table S4
Experimental models: Cell lines		
Normal Human Astrocytes	Lonza	Cat# CC-2565
MRC5	ATCC	CCL-171
Experimental models: Organisms/strains		
BALB/c nude mice	Animal Resources Centre, Australia	https://www.arc.wa.gov.au/
NOD/SCID mice	Animal Resources Centre, Australia	https://www.arc.wa.gov.au/
Software and Algorithms		
ImageJ	NIH	https://imagej.nih.gov/ij/
Calcusyn	Biosoft	http://www.biosoft.com/w/calcusyn.htm
Graphpad Prism 6	Applied BioSystems	https://www.graphpad.com
Partek Genomics Suite Analysis Software	Partek	https://www.partek.com
R packages limma	Ritchie et al., 2015	http://bioconductor.org/packages/release/bioc/html/limma.html
Biorender	Biorender	https://biorender.com

RESOURCE AVAILABILITY

Lead contact
Further information and requests for resources and reagents should be directed to Associate Professor David S. Ziegler, d.ziegler@unsw.edu.au.

Materials availability
This study did not generate novel reagents.

Data and code availability
The microarray data for the effect of CBL0137 on HSJD-DIPG007 cells are available at Gene Expression Omnibus database [GEO: GSE153883/ https://www.ncbi.nlm.nih.gov/geo/query.acc.cgi?acc=GSE153883].

The microarray data for the combination of CBL0137 and panobinostat on HSJD-DIPG007 cells are available at Gene Expression Omnibus database [GEO: GSE153441/ https://www.ncbi.nlm.nih.gov/geo/query.acc.cgi?acc=GSE153441].

EXPERIMENTAL MODEL AND SUBJECT DETAILS

Cell culture models

Primary DIPG cultures (SU-DIPGs and HSJD-DIPGs) were kindly provided by our collaborators at Stanford University (USA) and St John of Hope Hospital (Spain) respectively. The AUS-DIPG017 culture was developed as part of the HoTRods autopsy study as described at (Tsoli et al., 2018). The cells were cultured in DMEM/F12 and Neurobasal media (1:1) supplemented with HEPES, non-essential amino acids, antibiotic/antimycotic, pyruvate, glutamax, heparin, B27, human EGF, human FGF, PDGF-AA and PDGF-BB. Neurospheres were passaged weekly and their medium was changed every 3 days. Normal human astrocytes and MRC5 cells were purchased from Lonza, Australia, and grown according to the manufacturer's instruction. All cells were maintained at 37°C in 5% CO_2 and humidified atmosphere.

Animal models

All animal experiments were performed in accordance with the Animal Care and Ethics Committee of the University of New South Wales and the Australian Code of Practice for Care and Use of Animals for Scientific Purposes. All mice were maintained in a temperature-controlled environment with a 12 hour light/dark cycle. DIPG orthografts were generated as previously described (Tsoli et al., 2018). Briefly, female NOD/SCID and female balb c/nude mice (7-8 weeks, Animal Resources Centre, Perth, Australia) were stereotactically injected with 200,000 HSJD-DIPG007 or SU-DIPGVI in 2ul of matrigel in the 4th ventricle/pons. Animals were monitored daily for weight loss and neurological symptoms. If ataxia, circling, head tilting and/or weight loss of > 20% occurred, the mice were humanely euthanised.

METHOD DETAILS

High-throughput drug screening and cell viability assays

High-throughput screening (HTS) was performed on SU-DIPGVI cells cultured as neurospheres. Cells were seeded in either 96-well black assay plates (Corning) as single-cell suspensions using a Multidrop Combi dispenser (Thermo Fisher Scientific). Plates were incubated at 37°C and 5% CO_2 in a humidified environment under ambient conditions. DIPG cells were incubated for 72h and then treated with test and control compounds using a Hamilton STAR liquid handling robot equipped with a pin tool dispensing device. A collection of 3600 compounds were assembled from the following libraries the Prestwick Chemical Library, LOPAC library (Sigma) and the Tocri Screen Total library. Library compounds were tested at a final assay concentration of 10μM. After 72h drug exposure, cell viability was measured using the Alamar Blue assay with a PerkinElmer EnSpire plate reader. Data analysis was performed using the Activity Base (IDBS) software suite. The raw test data were normalized to negative control (DMSO only) for calculation of percent survival for each data point.

For cell viability assay, DIPG cells were seeded into 96-well plates (100 μL per well) and incubated for 72 hours to form neurospheres while NHAs and MRC5 cells were incubated for 24 hours prior to adding the drugs. After incubation, cells were treated with various concentrations of CBL0137 and panobinstat for an additional 72 hours. Resazurin reduction was then used to measure cell viability. Synergistic drug interactions were determined using CalcuSyn software (Biosoft) developed by Chou and Talalay where CI values of less than 1 indicated synergism, CI values more than 1 showed antagonism and CI equal to 1 represented additive effect. IC_{50} values were determined by non-linear regression analysis by Graphpad Prism 6 software (Applied BioSystems).

Clonogenic assay

Clonogenic assays were used to assess the effects of CBL0137, panobinostat and FACT knockdown on the clonogenic activity of DIPG cells. 24-well plates were coated by media containing 0.5% soft agar. After 24 hours, cell suspensions in media containing 0.33% agar and drugs or DMSO as a vehicle were added to the bottom layer. Depending on the growth rate of DIPG cultures, 1000-2000 cells were seeded in each well. Cells were maintained at 37°C in a humidified 5% CO_2 atmosphere. After 2-3 weeks, the colonies were stained using 5mg/ml 3-(4,5-dimethylthiazol-2-yl)-2,5-diphenyltetrazolium bromide (MTT) and counted using ImageJ software.

Western blot analysis

DIPG cells were lysed by using RIPA buffer supplemented with protease and phosphatase inhibitors and protein concentration was determined using the Pierce BCA Analysis Kit as per manufacturer's instructions. 30 μg protein was then incubated for 5 minutes at 95°C in Laemmli loading buffer containing 10% DTT (Bio-Rad). Electrophoresis was conducted at 80V for 2 hour and proteins were transferred to nitrocellulose membranes (BioRad) at 85V for 1 hour. Membranes were blocked in 5% skim milk in phosphate-buffered saline containing 0.05% Tween 20 (PBST) and then incubated with primary antibodies diluted in 5% bovine serum albumin in PBST containing overnight at 4°C [Ezh2 (1:1000, cell signaling #5246), SPT16 (1:1000, cell signaling #12191), SSRP1 (1:1000, cell signaling #13421), p16 (1:1000, cell signaling #80772), E2F1 (1:1000, cell signaling #80772), anti-gamma H2A.X (1:1000, abcam #ab26350), Rb (1:1000, cell signaling #9313), Phospho-Rb (1:1000, cell signaling #8516), GAPDH (1:2000, cell signaling #2118), β-Actin(1:1000, cell signaling #8457), CDK4 (1:1000, cell signaling #12790), H3K27me3 (1:1000, cell signaling #9733), H3K27ac (1:1000, cell signaling

#8173)]. Membranes were then washed 5x using PBST and incubated with secondary antibody in PBST for 1 hour at room temperature. Proteins were visualized by chemoluminescence (Super Signal, Pierce).

Apoptosis assay

HSJD-DIPG007 cells were seeded as 300,000 cells/well in laminin coated 6-well plate. After 24 hours incubation, cells were treated with either DMSO or various concentrations of CBL0137 for 48 hours. Cells were washed twice with cold PBS and resuspended in 100 μl of 1X Binding Buffer, 5 μl of FITC-Annexin V and 5 μl 7-AAD and incubated for 15 min at room temperature in the dark. After adding 400 μl of 1X Binding Buffer to each sample, the cells were analyzed by BD FACSCanto. Unstained untreated cells, FITC-Annexin V and 7-AAD single staining cells were used to set up compensation and quadrants.

shRNA-expressing lentivirus preparation

shRNA expressing lentiviral constructs against human *SSRP1 and SPT16 with* ViraPower Lentiviral Packaging Mix (a mixture of the pLP1, pLP2, and pLP/VSVG plasmids) were co-transfected into 293FT cells using Lipofectamine 2000 to generate lentiviral particles. Lentiviral particles were concentrated using polyethylene glycol (PEG) precipitation method. The precipitated lentiviruses were resuspended in PBS and stored at −80°C. For lentiviral infection, HSJD-DIPG007 cells were incubated with shRNA expressing lentivirus for 16 h. 48 h after infection, puromycin (0.5 μg/ml) was added to select virally infected cells for further experiments.

Co-immunoprecipitation assay

HSJD-DIPG007 and VUMC-DIPG10 cells were harvested, washed 1x with PBS and centrifuged at 1500RPM for 5 minutes. The cells were resuspended in low salt buffer (0.01M HEPES, 0.05M NaCl, 0.001M EDTA, 0.001M DTT, protease inhibitor, phosphatase inhibitor) and centrifuged at 1500RPM for 5 minutes. Cells were then resuspended in low salt buffer and incubated on ice for 15 minutes. After incubation, an equal volume of low salt buffer containing 0.4% NP-40 was added and the cells were incubated for 15 minutes on a rotary wheel at 4°C and centrifuged at 3000RPM for 5 minutes at 4°C. The pellet containing nuclear fraction was resuspended in high salt buffer (0.01M HEPES, 0.42M NaCl, 0.001M EDTA, 0.001M DTT, protease inhibitor, phosphatase inhibitor), vigorously resuspended and incubated for 30 minutes at 4°C. After centrifugation at high speed for 20 minutes at 4°C, the supernatant was collected, and protein concentrations were determined using BCA assay.

For pre-clearing and IP reaction, lysate concentrations were adjusted to 1μg/μl by no salt buffer [0.01M HEPES, 0.001M EDTA, protease inhibitor, phosphatase inhibitor; added to adjust high salt buffer (0.42M) down to isotonic level (0.15M)] and isotonic salt buffer (0.01M HEPES, 0.15 NaCl, 0.001M EDTA, 0.001M DTT, protease inhibitor, phosphatase inhibitor). Pre-clearing beads were washed 4x in bead wash buffer (0.01M HEPES, 0.15M NaCl, 0.001M EDTA, protease inhibitor, phosphatase inhibitor) for 5 minutes at room temperature. Tubes were then placed on magnet for 1 minute, the wash buffer was discarded, and isotonic lysate was added to the beads. The tubes were then incubated for 1 hour on rotary wheel at 4°C.

Protein A Dynabeads were resuspended in antibody/TBST solution (5μg IgG and H3K27M/1 mg dynabeads) and incubated for 15 minutes at room temperature. The beads were then washed in PBST and resuspended in conjugation buffer (20mM NaPO4, 0.15M NaCl - pH 7.5). Ab-bound beads were then resuspended in 5mM bis(sulfosuccinimidyl)suberate crosslinker followed by incubation at room temperature for 30 minutes. The reaction was then quenched using 1M Tris-HCl (pH 7.5) and the crosslinked beads (IgG, H3K27M) were washed by PBST. The beads were then collected on magnet and pre-cleared lysates (1μg/μl protein) were added to the beads and incubated overnight at 4°C. After incubation, beads were collected and washed 4x in post-IP wash buffer (0.01M HEPES, 0.15 NaCl, 0.001M EDTA, protease inhibitor, phosphatase inhibitor, 0.5% NP-40) for 3 minutes at room temperature followed by resuspension in post-IP wash buffer. The beads were then collected on magnet and Laemmli loading buffer containing 10% β-mercaptoethanol was added. After boiling at 90°C for 10 minutes, loading buffers containing eluted proteins were collected. The elutes subjected to western blot analysis as described above.

Enzyme-linked immunosorbent assay (ELISA)

HSJD-DIPG007 cells were treated with 600nM CBL0137 and 20nM panobinostat as single agents and in combination for 24 hours. Cells were washed with PBS and histone and DNA was extracted from the cells using Histone Extraction Kit (Abcam; Cat# ab113476) or Genomic DNA Extraction Kit (Abcam; Cat# ab156900). 100ng histone extract or DNA was subjected to ELISA assay for global acetyl histone H3K27, global histone H3 acetylation, global tri-methyl histone H3K27 and global DNA methylation according to the manufacturer's instruction (EpiQuik; Cat #P-4059, P-4008, P-3042, P-1034)

RT^2 Profiler PCR array and real-time PCR

HSJD-DIPG007 cells were treated with 600nM CBL0137 and 20nM panobinostat as single agents and in combination for 24 hours. Cells were washed with PBS and RNA was extracted using the RNeasy kit (QIAGEN) according to the manufacturer's instruction. RNA levels were quantified using an ND-1000 spectrophotometer (NanoDrop). cDNA was synthesized from 1 μg of RNA using RT2 First Strand Kit and 100ng of cDNA was used for RT^2 Profiler PCR Array specific for cell cycle and polycomb complex and oligodendroglial lineage genes. Real-time PCR was performed using ABI-7500 Real Time PCR System (Life Technologies). Relative mRNA

levels were determined by the comparative threshold cycle method using six housekeeping genes as controls for RT[2] Profiler PCR Array and four housekeeping genes for oligodendroglial lineage genes (Table S4).

Affymetrix gene expression analysis

HSJD-DIPG007 cells were treated for 24 hours with DMSO or 0.5μM CBL0137 as single agent. For combination therapy experiment, the cells were treated for 24 hours with DMSO, 0.6μM CBL0137, 20nM panobinostat and the combination of the two agents. After incubation, cells were harvested and washed 2x with PBS. RNA was then extracted using the RNeasy extraction kit (QIAGEN) according to the manufacturer's instruction. Gene expression data was obtained through the Affymetrix Clariom D Human microarray platform, containing 6,281,169 probes and 40,899 probesets. Probesets were processed using the Robust MultiArray (RMA) pipeline (PMID 21070630) followed by probeset annotation to gene symbols using the Bioconductor AnnotationDbi pipeline (PMID 16939789).

Immunohistochemistry

Excised brain tissues were fixed in formalin, embedded in paraffin and 5 μm sections were cut and mounted on Superfrost slides. The slides were dried in a 60°C oven for 1 hour and deparaffinised in xylene for 20 minutes. Slides were then re-hydrated with 100%, 90%, 70% ethanol, and MilliQ water. Antigen retrieval was performed by immersing the slides in 100 mM tri-sodium citrate buffer at pH 6 and heating for 20 minutes with a cooling interval of 10 minutes following every 5 minutes of heating. The endogenous peroxidases were then inactivated by immersing the slides in 3% hydrogen peroxide. Non-specific binding of immunoglobulin was blocked by 2.5% bovine serum albumin, 2.5% fetal calf serum, and 0.2% Triton-X for 1 hour at room temperature. Slides were then incubated with primary antibodies [SSRP1 (1:1000, Origene #TA308461), SUPT16H (1:1000, Thermo Fisher Scientific #MA5-27214), Ki67 (1:1000, Abcam #ab209897), H3K27me3 (1:500, Abcam #ab6002), H3K27ac (1:500, Abcam #ab177178)] at 4°C overnight followed by incubation with secondary antibodies for 1 hour at room temperature. Finally, the slides were washed in MilliQ water and dehydrated sequentially with 70%, 90%, and 100% ethanol.

In vivo drug treatment

For single agent study, NOD/SCID mice received 50 mg/kg CBL0137 prepared in 5% dextrose intravenously, once a week for four weeks. Treatment started 4 weeks post intracranial HSJD-DIPG007 cells inoculation and upon drug treatment, the animals were given mushy food as a supplement to prevent weight loss and dehydration. In a separate experiment, CBL0137 was administered intravenously at 20 mg/kg/day in a 5 days on, 2 days off schedule for 2 weeks. Mice in control groups received 5% dextrose.

For the combination study on HSJD-DIPG007 in NOD/SCID mice, CBL0137 was prepared as described above and given intravenously at 50 mg/kg once a week for four weeks. For SU-DIPGVI animal model in BALB/c nude mice, drug treatment started 9 weeks after the surgery. CBL0137 was administered at the dose of 40 mg/kg every four days for four weeks. In both studies, panobinostat was dissolved in 2.5% DMSO, 5% PEG400 and 5% Tween80 in 0.9% saline and administered intraperitoneally at the dose of 10 mg/kg, M,W,F for four weeks in HSJD-DIPG007 model. For SU-DIPGVI model panobinostat was given at 5 mg/kg/day, 5 days on, 2 days off for four weeks. Control animals received the vehicles of both drugs.

LC-MS/MS determination of CBL0137 concentration in blood and tissue samples

Female NOD/SCID mice were injected with 2 × 10^{5} HSJD-DIPG007 in 2ul of Matrigel intracranially. Four weeks later, a single 20 mg/kg or 50 mg/kg dose was administered intravenously to mice and blood and brain tissue samples collected at 30 min, 1, 2, 4, 8, 24, 48 and 72 hours after injection. Sample preparation: The samples were prepared for analysis using a methanol extraction procedure. Approximately 100 mg sections of tumor tissue were supplemented by methanol 1:10 (wt:vol) containing 0.1% formic acid and homogenized using a hand held homogenizer. To complete the compound extraction, the sample solutions were rocked overnight at 2-8°C and then centrifuged for 10 minutes at 14000 rpm and 2-8°C to precipitate the homogenized tissue pellet. The supernatant was then separated and diluted 1:4 (vol/vol) with mobile phase A (MPA) and analyzed by LC-MS/MS versus a reagent-matched calibration curve. Plasma samples were prepared by 1:4 (vol/vol) methanol extraction followed by vortexing for 5 minutes. The samples were then centrifuged for 10 minutes at 14,000 rpm and 2-8°C to precipitate the proteins and the supernatant was collected.

LC-MS/MS instrument: The Thermo Fisher TSQ Quantum LC-MS/MS system was used for pharmacokinetic analysis using Phenomenex Kinetex 1.7u C18, 100A, 2.1 × 50mm column with a flow rate: 0.6 mL/min at 25°C. The auto-sampler cooling block temperature was set at 4°C and the injection volume was 10 μl. Mobile phase A was contained of 0.1 formic acid in water and mobile phase B was consisted of 0.1% formic acid in acetonitrile. A gradient mobile phase was initiated with 90% mobile phase A and 10% mobile phase B to 90% mobile phase B and 10% mobile phase A at 2.01 min. The gradient remained constant for 4 min at which time, it was changed linearly to 90% mobile phase A and 10% mobile phase B at 6.01 min until the end of the run.

Calibration was calculated by least-squares analysis. The calculation used the peak area of the calibration standards versus the concentrations of the calibration standards. The concentration of CBL0137 in the study samples was calculated using the calibration curve established by the calibration standards. CBL0137 concentration was expressed in μg/mL, assuming 1 mg/mL density of tumor tissue.

QUANTIFICATION AND STATISTICAL ANALYSIS

All statistical analyses were performed using GraphPad Prism 6 software. For *in vitro* and immunohistochemistry experiments, two-way ANOVAs (Tukey's test and Dunnett's multiple comparison test) were used. For survival analyses of orthotopic xenografts, a Log-rank (Mantel-Cox) test was employed. Bioinformatic analyses were performed using Partek Genomics Suite and R packages limma (Ritchie et al., 2015) and ruv (Molania et al., 2019). Images were analyzed using ImageJ Software (ImageJ, Maryland, USA). p values < 0.05 were considered statistically significant.